



1 Land-atmosphere interactions in the tropics

2

3 Pierre Gentine

4 *Department of Earth and Environmental Engineering,*

5 *Earth Institute*

6 *Columbia University, New York, USA*

7

8 Adam Massmann

9 *Department of Earth and Environmental Engineering,*

10 *Earth Institute,*

11 *Columbia University, New York, USA*

12

13

14 Benjamin R. Lintner

15 *Department of Environmental Sciences*

16 *Rutgers, The State University of New Jersey*

17 *New Brunswick, NJ, USA*

18

19 Sayed Hamed Alemohammad

20 *Department of Earth and Environmental Engineering,*

21 *Earth Institute,*

22 *Columbia University, New York, USA*

23

24 Rong Fu

25 *Atmospheric and Ocean Sciences Department*

26 *University of California, Los Angeles*

27



28 Julia K. Green

29 *Department of Earth and Environmental Engineering,*

30 *Earth Institute,*

31 *Columbia University, New York, USA*

32

33 Daniel Kennedy

34 *Department of Earth and Environmental Engineering,*

35 *Earth Institute,*

36 *Columbia University, New York, USA*

37

38 Jordi Vilà-Guerau de Arellano

39 *Meteorology and Air Quality Group*

40 *Wageningen University, Wageningen, the Netherlands*

41

42

43

44

45

46

47

48 *Corresponding author address:* Pierre Gentine, Department of Earth and Environmental
49 Engineering, Columbia University, NY 10027, USA.

50 E-mail: pg23288@columbia.edu

51 Phone number: +1-212-854-7287

52

53

54



55 ABSTRACT

56

57 The continental tropics play a leading role in the terrestrial water and carbon cycles. Land-
58 atmosphere interactions are integral in the regulation of surface energy, water and carbon fluxes
59 across multiple spatial and temporal scales over tropical continents. We review here some of the
60 important characteristics of tropical continental climates and how land-atmosphere interactions
61 regulate them. Along with a wide range of climates, the tropics manifest a diverse array of land-
62 atmosphere interactions. Broadly speaking, in tropical rainforests, light and energy are typically
63 more limiting than precipitation and water supply for photosynthesis and evapotranspiration;
64 whereas in savanna and semi-arid regions water is the critical regulator of surface fluxes and
65 land-atmosphere interactions. We discuss the impact of the land surface, how it affects shallow
66 clouds and how these clouds can feedback to the surface by modulating surface radiation. Some
67 results from recent research suggest that shallow clouds may be especially critical to land-
68 atmosphere interactions as these regulate the energy budget and moisture transport to the lower
69 troposphere, which in turn affects deep convection. On the other hand, the impact of land surface
70 conditions on deep convection appear to occur over larger, non-local, scales and might be
71 critically affected by transitional regions between the climatologically dry and wet tropics.

72 1 Introduction

73 Tropical ecosystems play a substantial role in regulating the global carbon and hydrologic
74 cycles. Tropical rainforests are one of the main terrestrial carbon sinks [Nakicenovic,
75 2000] but their projected response to a warming climate remains unclear because of
76 uncertainties associated with the representation of abiotic and biotic processes in models
77 as well as confounding factors such as deforestation and changes in land use and land
78 cover [Wang *et al.*, 2009; Davidson *et al.*, 2012; Fu *et al.*, 2013; Saatchi *et al.*, 2013;
79 Hilker *et al.*, 2014; Boisier *et al.*, 2015; Doughty *et al.*, 2015; Gatti *et al.*, 2015; Knox
80 *et al.*, 2015; Saleska *et al.*, 2016]. The ecosystems of tropical monsoonal and seasonal wet-
81 dry climates are also important contributors to the global carbon cycle, especially with
82 respect to the interannual variability of the tropical terrestrial carbon sink [Poulter *et al.*,
83 2014; Jung *et al.*, 2017].

84 Some regions of the tropics have been further identified as hotspots of land-atmosphere
85 interactions, modifying the regional climate [Green *et al.*, 2017] either locally, i.e. at
86 horizontal scales on the order of a few boundary layer heights, regionally, at scales up to



87 a few hundreds of kilometers, or at large scales, over several of thousands of kilometers,
88 through coupling between the surface and the overlying atmosphere [*Lintner and Neelin,*
89 2009]. While tropical land-atmosphere interactions are often examined through the lens
90 of coupling between land surface states (e.g., soil moisture) and rainfall, other aspects of
91 the coupling are also important. For example, even under nonprecipitating conditions,
92 surface radiation, temperature and vapor pressure deficit (VPD) may be altered [*Lawton*
93 *et al.*, 2001; *Pielke et al.*, 2016; *Green et al.*, 2017] through coupling with clouds,
94 aerosols and shallow (non-precipitating) convection [*Avissar and Nobre*, 2002; *Medvigy*
95 *et al.*, 2011; *Seneviratne*, 2013; *Cook et al.*, 2014; *Guillod et al.*, 2015; *Krakauer et al.*,
96 2016; *Martin et al.*, 2016; *Green et al.*, 2017; *Khanna et al.*, 2017; *Martin et al.*, 2017;
97 *Thiery et al.*, 2017; *Vogel et al.*, 2017]. It is clear that the tropical energy, water, and
98 carbon cycles cannot be understood in isolation; rather, interactions among these cycles
99 are critical, especially in determining whether the terrestrial tropics will act as a future
100 carbon sink or source [*Zhang et al.*, 2015][*Swann et al.*, 2015].

101 The two-way interactions that occur between the land surface and overlying atmosphere
102 represent one of the more uncertain aspects of the terrestrial climate system, particularly
103 in the tropics [*Betts and Silva Dias*, 2010]. While the land surface is widely recognized as
104 integral to the occurrence of important tropical climate phenomena such as monsoons
105 [*Zeng and Neelin*, 1999; *Zeng et al.*, 1999], isolating and quantifying its precise role
106 remains elusive. Indeed, such efforts have frequently been hampered by the paucity of
107 observational data, not to mention the complex and multiple pathways through which
108 land-atmosphere interactions can take place.

109 Several field campaigns have been conducted in the tropics with the purpose of
110 advancing knowledge of land-atmosphere interactions. One of the first campaigns was
111 the Large-Scale Biosphere-Atmosphere Experiment in Amazonia (LBA) [*Avissar et al.*,
112 2002; *Keller et al.*, 2004], which aimed at refining our understanding of climatological,
113 ecological, biogeochemical and hydrological processes of the Amazon and their linkages,
114 in addition to the anthropogenic impacts (e.g., land-use land cover changes and
115 deforestation, in particular) on these. Among many other topics, LBA generated
116 fundamental insights on the structure of the tropical atmosphere, processes generating
117 precipitation, and the seasonal variability of rainforest surface turbulent fluxes [*Avissar*
118 *and Nobre*, 2002; *Betts et al.*, 2002; *Laurent et al.*, 2002; *Machado and Laurent*, 2002;



119 *Acevedo et al.*, 2004; *Khairoutdinov and Randall*, 2006; *Fitzjarrald*, 2007; *Juárez et al.*,
120 2007; *Restrepo-Coupe et al.*, 2013]. Much of the initial LBA research attempted to isolate
121 the effect of deforestation on precipitation, both in a local context as well as remotely via
122 teleconnections [*Avissar et al.*, 2002]. Much of this research pointed to deforestation
123 decreasing precipitation, albeit with uncertain magnitude. Even now, two decades after
124 the inception of LBA, the relationship between tropical deforestation and precipitation
125 remains uncertain, despite progress with respect to key processes such as the forest's role
126 in accessing deep water in the dry season, and cloud-cover's role in modulating energy
127 availability for photosynthesis [*Betts and Dias*, 2010].

128 Another noteworthy field campaign, the African Monsoon Multidisciplinary Analysis
129 (AMMA) campaign, focused on the West African monsoon system, especially the Sahel
130 transition zone [*Redelsperger et al.*, 2006; *Boone et al.*, 2009b]. AMMA built upon
131 previous field work in the region [*e.g. HAPEX-Sahel, Gourtorbe et al. 1993*], and
132 substantially advanced understanding of mesoscale convective systems and their
133 initiation the role of surface processes, and the vegetation water stress response in semi-
134 arid regions [*Lebel et al.*, 2009; *Taylor et al.*, 2009; *Boone et al.*, 2009a; *Lohou et al.*,
135 2010; *Couvreux et al.*, 2011a; 2011b]. More recently, the 2014-2015 Green Ocean
136 Amazon (GO-Amazon) campaign [*Martin et al.*, 2016] sought to quantify the impact of
137 atmospheric composition and aerosols under clean and polluted conditions on cloud
138 formation and radiation over the basin, as well as on shallow to deep convection
139 development [*Anber et al.*, 2015a; *Tang et al.*, 2016; *Giangrande et al.*, 2017].

140 The remainder of this review article is organized as follows. We first review the typical
141 definitions of the tropics and of land-atmosphere interactions in section 2. In section 3 we
142 discuss the seasonality and characteristics of the climate of the tropics. The different
143 types of feedbacks from local to non-local (i.e. remote influences) are then highlighted in
144 section 4, and we close in arguing that shallow cloud feedback and its impact on radiation
145 has received too little attention compared to precipitation feedback, in rainforests
146 especially.



147 2 Definitions of land-atmosphere interactions in the tropics

148 2.1 What (where) are the Tropics?

149 There exist multiple definitions of the Tropics. On the one hand, the Tropics can be
150 defined spatially as the area between the Tropics of Cancer and Capricorn, located at
151 $\sim 23\frac{1}{2}^{\circ}$ N and $\sim 23\frac{1}{2}^{\circ}$ S, respectively. On the other hand, it is sometimes useful to define
152 the Tropics in terms of underlying climate or physical characteristics. One such
153 physically-motivated definition of the Tropics is the region over which mean top-of-the-
154 atmosphere solar incoming radiation exceeds outgoing radiation (reflected shortwave and
155 outgoing longwave), which occurs equatorward of $\sim 35^{\circ}$. Another definition is the region
156 near the equator where the Coriolis effect is small and planetary scale equatorial wave
157 dynamics are dominant, which strongly affects the dynamics, as we elaborate below
158 [Sobel *et al.*, 2001; Sobel and Bretherton, 2003; Lintner and Chiang, 2005; Raymond and
159 Zeng, 2005].

160 Over land, the Tropics are often defined biogeographically, as in the traditional Köppen
161 climate classification scheme [Köppen, 1884]: tropical regions are divided into three
162 main groups—tropical rainforest, tropical monsoon, and tropical wet and dry (or
163 savanna)—all of which are characterized by annual mean temperatures exceeding 18°C
164 but which differ in terms of precipitation amount and seasonality.

165 The latitudes between the Tropics of Cancer and Capricorn encompass some regions of
166 large-scale subsidence and limited rainfall, including drylands and deserts, which we
167 largely neglect here, even though land-atmosphere coupling processes within these
168 regions is clearly of interest. Thus, throughout this manuscript, we define the Tropics as
169 the latitudinal band between -15° S and 15° N, as it captures most of the wet regions of
170 the Tropics while excluding many of the more arid regions at higher latitudes.

171 2.2 How to define land-atmosphere interactions?

172 There are typically two main definitions of land-atmosphere interactions:

173 2.2.1 Surface turbulent fluxes

174 While many potential definitions of land-atmosphere interactions exist, we propose a
175 definition of land-atmosphere interactions as the study of turbulent fluxes and associated
176 momentum, energy, water and trace gases exchanges between the biosphere and the



177 atmosphere [Goulden *et al.*, 2004; Fisher *et al.*, 2009; Restrepo-Coupe *et al.*, 2013].
178 Surface turbulent flux measurements in the tropics are usually obtained from eddy-
179 covariance methods, typically above the canopy [Baldocchi *et al.*, 2001]. Observing
180 turbulent fluxes is challenging in tropical environments for many reasons including
181 logistics, maintenance and the harsh environment such as intense rainfall, high wind, and
182 relative humidity, which impacts the sensors [Campos *et al.*, 2009; Da Rocha *et al.*,
183 2009; Restrepo-Coupe *et al.*, 2013; Zahn *et al.*, 2016; Chor *et al.*, 2017; Gerken *et al.*,
184 2017]. In light of these challenges, it is perhaps not surprising that even the best estimates
185 of surface turbulent fluxes manifest large uncertainties [Mueller *et al.*, 2011].
186 Apart from site level measurements, remote sensing observations can provide
187 information about surface turbulent fluxes and other relevant quantities over tropical land
188 regions. There is considerable uncertainty in upscaling point observations to larger areas.
189 Remote sensing observations are useful to generalize and compare fluxes across the
190 tropics even if they are not as direct as point observations, which are limited to ~ 10 local
191 stations across the wet tropics. We emphasize that there are considerable uncertainties in
192 remote sensing and reanalysis estimates of rainfall [Washington *et al.*, 2013; Levy *et al.*,
193 2017], radiation [Jimenez *et al.*, 2011], and surface turbulent fluxes [Alemohammad *et al.*,
194 2016].
195 While direct, satellite-based retrievals of turbulent fluxes of carbon (i.e. gross primary
196 production (GPP)) and water would be most suitable for the study of tropical land-
197 atmosphere interactions, such retrievals are beyond current remote sensing capability.
198 However, some recent work demonstrates that existing satellite observations may still be
199 leveraged to study surface turbulent fluxes in the tropics. Alemohammad *et al.* [2016]
200 applied a machine learning algorithm based on remotely-sensed Solar-Induced
201 Fluorescence (SIF), called WECANN (Water Energy and Carbon Artificial Neural
202 Network) to derive surface turbulent fluxes. WECANN reproduces the seasonality in the
203 wet tropics and exhibits plausible interannual. In contrast to the normalized difference
204 vegetation index (NDVI) or many other vegetation indices which are indirect byproducts
205 of photosynthesis, SIF (at the leaf scale) is directly related to the ecosystem-scale
206 photosynthesis rate, providing important information on the impact of stressors on
207 photosynthesis and is available from existing remote sensing platforms [Frankenberg *et al.*,
208 *et al.*, 2011; Joiner *et al.*, 2011; Frankenberg *et al.*, 2012; Joiner *et al.*, 2013; Frankenberg



209 *et al.*, 2014; *Guanter et al.*, 2014; *Lee et al.*, 2015; *Duveiller and Cescatti*, 2016; *Liu et*
210 *al.*, 2017; *Thum et al.*, 2017; *Alexander et al.*, n.d.]. SIF is thus an important indicator of
211 the rates of photosynthesis and transpiration through stomatal (small pores at the leaf
212 surface) opening [*Alemohammad et al.*, 2017]. Indeed, during photosynthesis plants take
213 up CO₂ from the atmosphere while releasing water to the atmosphere through stomata.
214 WECANN performs well compared to eddy-covariance observations and has less
215 uncertainty compared to many other retrievals (see [*Alemohammad et al.*, 2017]). We
216 note that recent developments in observations of SIF seem to indicate that the major
217 fraction of the SIF signal might be related to chlorophyll photosynthetically active
218 radiation and that changes in SIF yield (equivalent to light use efficiency) may account
219 for only a small fraction of the observed SIF signal [*Du et al.*, 2017]. This is still an open
220 topic to better understand what is actually observed by SIF remote sensing.

221 2.2.2 Weather and climate feedback

222 A second definition of land-atmosphere interactions relates to the feedback between
223 surface processes (radiation, surface turbulent fluxes) and the overlying atmosphere,
224 which may occur across multiple temporal and spatial scales. Throughout this
225 manuscript, we highlight contribution of three types of feedbacks:

- 226 1) feedbacks between the surface and low-level clouds, including surface fog and shallow
227 convection;
- 228 2) feedbacks between the surface and deep convection, i.e. deep raining clouds extending
229 above the freezing level;
- 230 3) feedbacks between the surface and large-scale circulation.

231 The distinction between shallow and deep convection remains elusive, as these have been
232 regarded as both fundamentally distinct or as a continuum, in both observations and
233 model convection parameterizations [*Khairoutdinov and Randall*, 2006; *Bretherton and*
234 *Park*, 2009; *Park and Bretherton*, 2009; *Rio et al.*, 2009; *Wu et al.*, 2009; *Del Genio and*
235 *Wu*, 2010; *Hohenegger and Bretherton*, 2011; *Böing et al.*, 2012; *D'Andrea et al.*, 2014;
236 *Rochetin et al.*, 2014b]. We will loosely refer to shallow convection as convection
237 confined below the freezing level (typically less than 3km deep) and comprising non-
238 precipitating clouds with motions of small scale (typically less than a km in the
239 horizontal).



240 An important point is that shallow convection is frequently generated by thermals rooted
241 in the boundary layer and is thus ultimately related to surface sensible (H) and latent heat
242 (LE) flux and their partitioning [Gentine *et al.*, 2013a; 2013b; de Arellano *et al.*, 2014].
243 The impact of surface heat fluxes and their partitioning on shallow convection is
244 demonstrated in the Amazon in **Figure 1**. Shallow convection frequently occurs over the
245 vegetated surface away from the ocean; also, over cooler and more humid river basins,
246 shallow clouds are virtually absent [Gentine *et al.*, 2013a; Rieck *et al.*, 2014; 2015]. In
247 addition, shallow convection is strongly influenced by the diurnal cycle of surface
248 radiation and surface turbulent heat fluxes [Gentine *et al.*, 2013a; 2013b; de Arellano *et*
249 *al.*, 2014].

250 On the other hand, we use the term deep convection in association with deep,
251 precipitating clouds. Deep convection may be triggered by boundary layer thermals
252 [D'Andrea *et al.*, 2014; Guillod *et al.*, 2014; Rochetin *et al.*, 2014a; 2014b; Anber *et al.*,
253 2015a] as well as other processes such as radiative destabilization [Anber *et al.*, 2015b],
254 meso- and large-scale circulations [Werth and Avissar, 2002; Roy *et al.*, 2003], cold pools
255 (cold density currents due to rain evaporation that cools the air within precipitating
256 downdrafts) [Engerer *et al.*, 2008; Del Genio and Wu, 2010; Böing *et al.*, 2012; Feng *et*
257 *al.*, 2015; Torri *et al.*, 2015; Gentine *et al.*, 2016; Heever, 2016; Drager and van den
258 Heever, 2017] and wave activity [Kuang, 2008; 2010]. As such, deep convection may be
259 viewed as less dependent on the surface state compared to shallow convection.

260 Over the central Amazon a large fraction of wet season precipitation occurs during the
261 nighttime (Figure 2). Moreover, during the daytime in both the dry and the wet seasons,
262 the diurnal cycle reflects not only locally surface-triggered deep convection
263 [Khairoutdinov and Randall, 2006; Ghate and Kollias, 2016] but also mesoscale
264 convective systems propagating on daily time scales throughout the Amazon basin
265 [Ghate and Kollias, 2016]. However, during the dry season, precipitation occurs more
266 frequently with the “popcorn type” deep convection that is more locally triggered and
267 thus directly related to the state of the land surface [Ghate and Kollias, 2016] (see an
268 example here <https://youtu.be/c2-iqzZziPU>).

269 Current generation climate models struggle to represent both shallow and deep
270 convection over continents [Guichard *et al.*, 2004; Bechtold *et al.*, 2013; Yin *et al.*, 2013;
271 D'Andrea *et al.*, 2014; Couvreur *et al.*, 2015], and especially in the tropics, as they



272 exhibit substantial errors in the phasing and intensity of both the diurnal and seasonal
273 cycles of convection [*Bechtold et al.*, 2013], as well as biases in the climatological
274 distribution of rainfall over land. For example, over the Amazon, many climate models
275 underestimate surface precipitation, evapotranspiration, and specific humidity [*Yin et al.*,
276 2013], with the dry bias in moisture extending upwards into the lower free troposphere
277 {Lintner:2017gm}. Such biases are largely thought to reflect deficiencies or errors in how
278 convection is represented in models [*Yano and Plant*, 2012; *Stevens and Bony*, 2013;
279 *Bechtold et al.*, 2014]. Indeed, in current generation climate models, cloud processes
280 occur at scales smaller than resolved grid-scale prognostic variables and therefore need to
281 be parameterized, i.e. represented as a function of the resolved-scale variables. This is
282 important as it means that climate models do not explicitly represent the small-scale
283 convective physics of the climate system. We do note, however, that cloud resolving
284 models which include explicit convection at scales of ~ 1 km alleviate many of the biases
285 observed in climate models, especially in terms of the diurnal cycle of convection or the
286 sign and magnitude of the feedbacks between deep convection and surface evaporative
287 fraction [*Taylor et al.*, 2013; *Anber et al.*, 2015a]. Nonetheless, due to convective wave
288 coupling in the Tropics, a simple prescription of lateral boundary conditions in small-
289 domain cloud-resolving model may be problematic, as the convective scales ultimately
290 interact and are coupled with the planetary scales. With a sufficiently large domain and
291 fine enough resolution, coupling between the convective scales and planetary scales may
292 be explicitly resolved, but simulations of this nature are likely too be computationally too
293 expensive for many applications. However, techniques exist to represent the effect of
294 large-scale dynamics on the convective scales, which, when combined with cloud
295 resolving simulations, yield powerful tools for understanding land-atmosphere
296 interactions in the tropics, as we elaborate further below.

297 3 Characteristics of the tropics

298 3.1 Weak temperature gradient approximation – nonlocality

299 One key concept in tropical climate is the Weak Temperature Gradient (WTG)
300 approximation. In the tropical free troposphere, horizontal gradients of temperature (and
301 pressure) are small in part because of the relative weakness of the Coriolis parameter (as



302 on large-scales, geostrophic balance holds poleward of ~ 5 degrees). Homogenization
303 occurs over a spatial scale comparable to the Rossby radius of deformation, which is
304 inversely proportional to the Coriolis parameter. In midlatitudes, the Rossby radius is of
305 order 10^2 km (similar to climate model resolution). In the tropics, the Rossby radius is
306 typically an order of magnitude larger. Consequently, localized convection, and the
307 diabatic heating associated with condensation and freezing of water, cannot be viewed in
308 isolation from the large-scale in the tropics: in other words, in the tropical free
309 troposphere, the temperature and pressure fields rapidly adjust to localized perturbations,
310 effectively spreading the effect of these perturbations. In addition, it is relatively
311 straightforward to show that adiabatic cooling, associated with large-scale vertical ascent
312 in the presence of a vertical gradient of dry static energy $h = c_p T + gz$, effectively
313 balances the diabatic heating rate Q , which in rainy regions of the tropics is mostly
314 associated with convective processes. This further emphasizes the coupling between
315 diabatic heating and large-scale ascent. Since the introduction of WTG, related and
316 refined frameworks, such as weak pressure gradient [Romps, 2012a; 2012b] or damped
317 gravity waves [Wang *et al.*, 2013], have been proposed. It should be emphasized that the
318 WTG framework is only valid in the free troposphere, above the boundary layer, as it
319 relates to wave dynamics in a stratified atmosphere.

320 The WTG framework has been used in single-column model and cloud-resolving models
321 of the tropics [Sobel *et al.*, 2007; Daleu *et al.*, 2012; 2014; Sentić and Sessions, 2017] to
322 obtain boundary conditions consistent with convective activity in the domain, thus
323 avoiding the issues of inconsistent boundary forcing alluded to in section 2.2.2. While the
324 WTG framework has often been applied in an oceanic context, [Anber *et al.*, 2015a] have
325 demonstrated its utility in studying the coupling between regional land surface processes
326 and larger-scale circulation, as discussed in Section XX.

327 3.2 Surface turbulent fluxes climatology and seasonality

328 Given that few flux towers are available across the tropics, we use WECANN
329 [Alemohammad *et al.*, 2017] to calculate surface flux climatologies across the continental
330 tropics. WECANN has been validated against available flux tower data and outperforms
331 other products in terms of reproducing both the seasonality and interannual variability
332 [Alemohammad *et al.*, 2017]. While remote sensing retrievals are not perfect and cannot
333 be considered the truth, they do provide spatially extensive data coverage, including



334 regions with sparse (or no) site-level measurements (e.g., Congo), which are hard to
335 upscale to larger scale. In what follows, we evaluate climatologies of evapotranspiration
336 (ET) and gross primary production (GPP) against precipitation (based on GPCP 1DD
337 v1.2 [Huffman *et al.*, 2001]) and net radiation (based on CERES SYN [Kato *et al.*, 2013])
338 (Figure 4 to Figure 8).

339 We first focus on the main tropical rainforests and the northeastern savanna (or Cerrado)
340 region of Brazil (Figure 4). In the wetter part of the Amazon, net radiation, R_n , peaks in
341 the dry season (August to November) (Figure 4) when precipitation and cloud cover—
342 especially shallow cloud cover, including fog—are reduced, [Anber *et al.*, 2015a]. As a
343 result of the reduced cloud cover, incident surface solar radiation increases, and both GPP
344 (Figure 6) and ET (Figure 7) increase in the dry season (Figure 4). As discussed further
345 in the next section, the forest in the climatologically wetter Amazon is primarily light
346 limited, while water stress there is moderate in the dry season. The seasonal cycle is more
347 pronounced for GPP than for ET (Figure 4), as canopy rain interception comprises a large
348 fraction of total ET in the wet season [Scott *et al.*, 1997; Oleson *et al.*, 2008; Miralles
349 *et al.*, 2010; Sutanto *et al.*, 2012; van Dijk *et al.*, 2015; Andreasen *et al.*, 2016] and partly
350 compensates for reduced transpiration in the wet season. In fact, because of this
351 compensation, the wettest parts of the Amazon exhibit weak ET seasonality. On the other
352 hand, most land-surface models exaggerate water stress in the Amazon [Powell *et al.*,
353 2013] and typically exhibit much lower rates of ET and GPP in the dry season, as well as
354 opposite seasonality of net ecosystem exchange, than are observed [de Gonçalves *et al.*,
355 2013; Alemohammad *et al.*, 2016; 2017].

356 In contrast to the everwet central Amazon, over the Cerrado region of Northeastern
357 Brazil, the seasonal cycles of R_n , precipitation, GPP and ET are much more pronounced,
358 with a marked dry season (Figure 4). The seasonal cycle of GPP tracks precipitation,
359 exhibiting a strong increase during the wet season. Similarly, ET increases sharply in the
360 wet season and then decreases more slowly than precipitation in the dry region (Figure
361 4). Conversely, net radiation increases sharply during the dry season. This region clearly
362 exhibits a strong water stress response.

363 Over the Maritime Continent, rainfall is intense throughout the year and seasonality is
364 modest, with a short peak in November to January (Figure 4). Much of the seasonal cycle
365 is attributable to monsoon circulations, which are strongly influenced by topography and



366 the land- and ocean-surface thermal contrast [Chang 2005]; however, the complexity of
367 the topography and the distribution of island land masses leads to strong local variability.
368 Additionally, the Madden Julian Oscillation, an important mode of climate variability in
369 in the tropical Indo-Pacific with a lifecycle of 30-90 days, strongly impacts rainfall on
370 intraseasonal timescales [Hidayat and Kizu, 2009]. Convective activity in the region also
371 regulates the East Asian Monsoon [Huang and Sun, 1992]. The region is also influenced
372 by topographic effects and land-sea breeze interactions at shorter time scales, and
373 exhibits a strong diurnal cycle in convection [Nitta, 1987; Hamada *et al.*, 2008]. Given
374 the relatively steady annual cycle of precipitation with regular convection, ET and GPP
375 remain relatively steady throughout the entire year, exhibiting minimal seasonality, in
376 this light limited environment (Figure 4).

377 The Congo basin exhibits two rainy seasons (Figure 4), with peaks in March-April-May
378 and September-October-November, related to seasonal changes in moisture convergence
379 due to the African Easterly jet and Intertropical Convergence Zone (ITCZ) over the
380 Atlantic [Washington *et al.*, 2013]. Throughout the year, monthly-mean precipitation is
381 much less than that observed over the Amazon or Indonesia. The seasonality of GPP and
382 ET, to a lesser extent, tracks that of precipitation, with substantial decreases during the
383 June to August dry season and even more pronounced reduction during the December to
384 February period. This seasonality in GPP and ET (Figure 4) suggests that the Congo
385 basin should exhibit substantially more water stress during dry seasons compared to the
386 Amazon or Indonesian rainforests (Guan *et al.* 2015).

387 Integrated over the entire tropical latitudinal band, precipitation is highest in DJF and
388 MAM when the wet season extends over most of the Amazon and adjacent savanna
389 regions (Figure 5). GPP is maximized during the wet season in South America, as GPP is
390 highest in the savanna regions while GPP over the rainforest is effectively seasonally
391 invariant (Figure 7). The seasonal pattern of ET resembles GPP (Figure 7), mostly
392 reflecting the seasonality of water availability in drier, water-limited regions and
393 increased radiation in the dry season in the wetter, more energy-limited portions of the
394 Amazon. The seasonal cycle of sensible heat flux (Figure 8) largely follows water stress,
395 especially in the rainforest where radiation remains high throughout the year, with an
396 increase during the dry season. Water stress is further evidenced in the evaporative
397 fraction, EF, the ratio of latent heat flux to latent and sensible heat fluxes (Figure 9).



398 Tropically-averaged EF does not evolve much reflecting seasonal variation in the
399 latitudinal peak in radiation and compensation of decreased canopy interception by
400 transpiration (because of increased net surface radiation) in the dry season. However, in
401 transitional and dry regions to the east, EF exhibits substantial seasonal variation between
402 the wet season, when it peaks, and the dry season. The surface moist static energy flux
403 (assuming sea level elevation) shows variations in SON and JJA but otherwise remains
404 steady across longitudes because of compensation between the increased H and reduced
405 ET. In the dry to wet transition, SON, moist static energy flux exhibits an interesting peak
406 at about -60 longitude (Figure 10) though the combined increase in radiation, due to
407 reduced cloudiness, inducing higher sensible heat flux and maintained high ET rates.

408 Over tropical Africa, the precipitation is highest in JJAS during the wet phase of the West
409 African Monsoon, with a secondary maximum in DJF corresponding to the Southern
410 African Monsoon (Figure 5). Similarly the latitudinal-averaged GPP and ET increase
411 during the West African Monsoon (Figure 6, Figure 7), accompanied by a strong
412 decrease in sensible heat flux (Figure 8). In DJF the southern African Monsoon displays
413 increased water flux (Figure 7) and photosynthesis tracking the increased rainfall (Figure
414 5). The Congo rainforest clearly exhibits two brief rainy seasons (Figure 4, Figure 9),
415 with peaks in March-April-May and September-October-November (Figure 4) and
416 displays substantial water stress and strong reduction in EF to values below 0.6 during
417 the dry season (Figure 9).

418 3.3 Rainforest water stress

419 One outstanding challenge in modeling tropical land regions is why do most
420 contemporary land-surface models incorrectly represent the wettest rainforest GPP and
421 ET rates, their seasonal cycles, and how they relate to water stress? Capturing this
422 accurately will help better understand the seasonal course of GPP and ET in the tropics.

423 In the wettest tropical forests, such as the western portion of the Amazon or Indonesia,
424 energy and light limit the rates of ET and GPP. It is thus natural to conclude that soil
425 moisture and water stress have only minor effects in such regions and thus that
426 precipitation variability would not matter much. In fact, there exist sharp vertical
427 gradients in the canopy (as well as at the surface of the soil in the dry season) in terms of
428 light and water availability (along with nutrient allocation) (Figure 3). Understory species
429 receive only a small amount of mostly diffuse light. However, water is not typically



430 limiting for low-canopy species. Moreover, because relative humidity is high and VPD is
431 low, leading to low stress on understory stomatal and ecosystem conductance [*Leuning,*
432 1995; *Leuning et al.*, 1995; *Wang and Leuning*, 1998; *Medlyn et al.*, 2011; 2012; *Heroult*
433 *et al.*, 2013].

434 On the other hand, top canopy species receive a large amount of radiation, especially in
435 the dry season, causing sunlit leaf warming and desiccation leading to heat and water
436 stress [*Jardine et al.*, 2014]. Leaf and xylem water status are regulated by the relative
437 demand of sap from transpiration, which depends on incoming radiation, temperature and
438 VPD. It also depends on the supply of sap to the leaves which is controlled by xylem
439 conductivity and reduced by cavitation in the xylem [*Martinez-Vilalta et al.*, 2014;
440 *Martinez-Vilalta and Garcia-Forner*, 2016]. To avoid leaf desiccation and xylem
441 cavitation (formation of air bubbles blocking the ascent of sap flow from the roots to
442 the leaves) stomatal closure is usually observed during peak daytime sunlight hours in
443 rainforest canopy species [*Brodribb*, 2003; *Pons and Welschen*, 2003; *Zhang et al.*,
444 2013]. This reduces the drop in leaf and xylem water potential and thus avoids important
445 leaf desiccation or xylem cavitation (Figure 12). This type of behavior with strong
446 stomatal regulation appears to be the norm in the wettest tropical forests [*Fisher et al.*,
447 2006; *Konings and Gentine*, 2016].

448 In tall canopy species the flow in the xylem from the roots is limited and cannot
449 sufficiently rehydrate the upper xylem and leaves, and it cannot be compensated by the
450 plant internal storage, whereby stomatal shutdown is inevitable to avoid desiccation and
451 xylem cavitation (Figure 12) [*Phillips et al.*, 1997; 2004; *Lee et al.*, 2005; *Oliveira et al.*,
452 2005; *Phillips et al.*, 2008; *Scholz et al.*, 2011; *Zeppel et al.*, 2014; *Konings and Gentine*,
453 2016]. In summary, water stress in tropical rainforest canopy species is not primarily due
454 to soil water stress but rather to the atmospheric demand and the build up of water stress
455 in the soil-plant continuum. Radiation, temperature and VPD are therefore essential for
456 tropical forests further emphasizing the importance of radiation and light on those forests.
457 Land-surface and ecosystem models, apart from a few exceptions [*Xu et al.*, 2016;
458 *Kennedy et al.*, 2017], do not represent plant hydraulics and typically only rely on an
459 empirical reduction of stomatal and ecosystem conductance, and therefore transpiration
460 and GPP, as functions of root-averaged soil moisture or water potential (e.g., [*Noilhan*
461 *and Planton*, 1989; *Sellers et al.*, 1996a; 1996b; *Ek*, 2003; *Boulet et al.*, 2007; *Gentine et*



462 *al.*, 2007; *Ngo-Duc et al.*, 2007; *Stoeckli et al.*, 2008; *Balsamo et al.*, 2009; *Boone et al.*,
463 2009a; *Bonan et al.*, 2011; *Lawrence et al.*, 2011; *Niu et al.*, 2011; *Bonan et al.*, 2012;
464 *Canal et al.*, 2014; *Han et al.*, 2014; *Naudts et al.*, 2014; *De Kauwe et al.*, 2015; *Chaney*
465 *et al.*, 2016; *Chen et al.*, 2016; *Haverd et al.*, 2016] among others). The root profile
466 averaging of soil moisture or water potential to define water stress exaggerates the impact
467 of surface drying, as in reality deeper roots may still effectively transport water to the
468 plant xylem even if surface roots experience dry conditions and therefore can maintain
469 overall high rates of GPP and transpiration.

470 The inclusion of plant hydraulics in tall canopy species leads to strong differentiation
471 between leaf (and upper xylem) and soil water potential (Figure 12) during midday,
472 especially in the dry season. Indeed, leaf and xylem water potentials substantially drop
473 because of the large transpiration rates through the stomata and because the xylem cannot
474 be instantaneously refilled due to the large flow drag in the elongated xylem. As a result,
475 plant hydraulics induce a shutdown of stomata during the day reducing the transpiration
476 rate near peak solar hours, also known as “midday depression,” in order to reduce
477 desiccation of the leaf and xylem. In addition, plant hydraulics also induces a natural
478 hydraulic redistribution of water in the root profile reducing dryness in the upper profile
479 in the dry season [*Lee et al.*, 2005; *Oliveira et al.*, 2005; *Domec et al.*, 2010; *Prieto and*
480 *Ryel*, 2014; *Kennedy et al.*, 2017], using deep root moisture rather than surface soil
481 moisture when needed, as the water flows down gradient of water potentials. This is
482 fundamentally different from typical parameterizations using average water stress of the
483 root water profile, which are oversensitive to surface water stress, in typical
484 parameterizations [*Kennedy et al.*, 2017]. Both of those effects lead to reduced sensitivity
485 to water stress [*Kennedy et al.*, 2017] and help maintain higher rates of transpiration
486 throughout the entire dry season [*Kennedy et al.*, 2017], whereas typical land surface
487 models overestimate water stress in the dry season [*de Gonçalves et al.*, 2013;
488 *Alemohammad et al.*, 2016; 2017].



489 4 Land-atmosphere interactions – local and nonlocal

490 4.1 Local feedback and heterogeneity – shallow clouds (fog and shallow
491 convection)

492 We suggest that that the most critical land-atmosphere feedbacks in tropical rainforests
493 involve shallow clouds and fog rather than deep convective clouds. Clearly, much of the
494 focus of tropical land-atmosphere interactions has been on feedbacks involving
495 precipitating deep convection, and the impact of heterogeneity on convective rainfall. On
496 the other hand, the coupling of the land surface to radiation has been relatively
497 understudied. Shallow clouds lead to reduced productivity and transpiration [*Anber et al.*,
498 2015a], yet the latter depends on cloud thickness as cumulus (shallow convection)
499 generate more diffuse light and can boost photosynthesis when they are not too thick
500 [*Ouwensloot et al.*, 2017]. Fog on the other hand, strongly diminishes the amount of light
501 received by the ecosystems. Fog [*Anber et al.*, 2015a] and shallow clouds [*Giangrande et*
502 *al.*, 2017] appear to be one of the primary differences between the dry and the wet season
503 (in addition to the preferential occurrence of nighttime mesoscale convective systems in
504 the rainy season, which are not directly relevant for land-atmosphere interactions
505 associated with daytime processes). Low-level cloudiness largely affects the surface
506 incoming radiation by reducing shortwave surface incoming radiation in the wet season,
507 especially in the morning [*Anber et al.*, 2015a; *Giangrande et al.*, 2017], which in turn
508 leads to strong reduction in GPP and ET. These clouds are also tightly connected to
509 surface processes and especially the surface energy partitioning. Indeed nighttime fog,
510 which often persists into the early daylight hours, is largely induced by longwave
511 temperature cooling, especially in the presence of evening rain in the wet season, which
512 generates dew formation [*Anber et al.*, 2015a]. Shallow clouds are themselves directly
513 forced by surface-generated thermals due to boundary layer processes [*de Arellano et al.*,
514 2014], and they are modified by the sensible and latent heat flux magnitude [*de Arellano*
515 *et al.*, 2014]. Shallow convection and low-cloud cover are also tightly connected to the
516 seasonality of the forest and to the diurnal cycle [*Anber et al.*, 2015a; *Tang et al.*, 2016;
517 *Giangrande et al.*, 2017].
518 Historically, the study of land-atmosphere interactions in the Tropics, and tropical
519 rainforests in particular, has emphasized effects of heterogeneity, especially due to



520 deforestation, on the generation of deep convection through mesoscale circulations (see
521 [Lawrence and Vandecar, 2015] for a complete review, as well as [Avisar and Pielke,
522 1989; Pielke and Avisar, 1990; Pielke et al., 1991; Dalu et al., 1996; Avisar and
523 Schmidt, 1998; Taylor et al., 2007; 2009; 2011; Rieck et al., 2015; Khanna et al., 2017]).
524 The hypothesis behind this is that deforestation reduces EF and surface roughness
525 [Khanna et al., 2017]. The associated increased buoyancy flux over the deforested areas,
526 mostly reflecting a shift toward increased sensible heating, induces mesoscale
527 circulations. These circulations enhance cloudiness through local buoyancy fluxes,
528 turbulent kinetic energy generation, and low-level moisture advection from adjacent
529 forested areas, thus providing all the key ingredients for moist convection generation
530 [Rieck et al., 2014; 2015]. It seems unlikely however that momentum roughness plays a
531 major role in this high radiation environment [Park et al., 2017], where circulations are
532 mostly buoyancy-driven. Instead, the heat and moisture roughness lengths [Park et al.,
533 2017] as well as leaf area index and stomatal conductance, which scales the magnitude of
534 the evapotranspiration flux, are the main players, in addition to changes in soil moisture
535 availability, for the circulation.

536 Induced mesoscale circulations and associated deep convection are clearly observable
537 with remote sensing observations [Khanna et al., 2017] and are more important in the dry
538 season [Khanna et al., 2017], when convection is more locally, and regionally, triggered
539 [Anber et al., 2015a; Ghate and Kollias, 2016]. Once precipitation occurs though, cold
540 pools, i.e., density currents induced by ice melt and evaporating rain in downdrafts,
541 dominate the surface-induced mesoscale circulation [Rieck et al., 2015], and reduce the
542 surface heterogeneity signal. In the wet season, the relative contribution of local forcing
543 to the total rainfall is small as the bulk of the precipitation is due to mesoscale convective
544 systems or larger-scale systems propagating throughout the basin, less tightly connected
545 to surface and boundary layer processes [Ghate and Kollias, 2016].

546 Even during the dry season, a large fraction of the Amazon and of Indonesia only
547 experience minimal water stress (Figure 9 and Figure 8) so that increased radiation
548 generates higher rates of photosynthesis (Figure 6) and ET (Figure 7) [Anber et al.,
549 2015a]. As such the radiation feedback of mesoscale-induced clouds may systematically
550 impact clearings and deforested regions (Figure 13) and are more systematic and longer
551 lasting than mesoscale-induced convective rainfall. Fewer studies have studied changes



552 in shallow clouds [Wang *et al.*, 2000; Lawton *et al.*, 2001; Chagnon *et al.*, 2004; Ray *et al.*,
553 *et al.*, 2006; Wang *et al.*, 2009; Pielke *et al.*, 2011; Rieck *et al.*, 2014; Anber *et al.*, 2015a],
554 even though the impact of changes in the surface energy partitioning and heterogeneity
555 on low-level clouds is clear and spatially systematic (Figure 1). Given the importance of
556 cloud cover on shortwave radiation and their importance for the differentiation between
557 the dry and wet seasons over wet tropical rainforests we believe that this low-cloud
558 feedback might be quite critical for rainforest ecosystem functioning. Indeed it was
559 pointed out by [Morton *et al.*, 2014; Anber *et al.*, 2015a; Morton and Cook, 2016] that
560 light changes between the dry and wet season due to changes in cloud cover were one of
561 the primary reasons for changes in the seasonality of surface fluxes, in addition to leaf
562 flush out [Lopes *et al.*, 2016; Saleska *et al.*, 2016]. We also note that the shading due to
563 low clouds reduces surface temperature and ecosystem respiration [Mahecha *et al.*, 2010;
564 Peterhansel and Maurino, 2011; Thornley, 2011; Hadden and Grelle, 2016; Ballantyne *et al.*,
565 *et al.*, 2017]. So, cloud-induced reductions in respiration can cancel reductions in
566 photosynthesis, such that the net effect of cloud shading on net ecosystem exchange is
567 unclear. In an academic study inspired in the thermodynamic characteristics in the
568 Amazonia, [Horn *et al.*, 2015] showed that coupling with the surface leads to a change in
569 the length scales that characterized clouds, and a reduction of the cloud life time. As a
570 result, there are larger populations of smaller shallow cumuli.

571 In addition to regulating radiative energy balance at the surface, [Wright *et al.*, 2017]
572 have shown that shallow convection transports moisture, provided by plants' transpiration,
573 from the atmospheric boundary layer to the lower troposphere during the late dry season and early dry to wet transition seasons (July-September). This mechanism, referred to as the "shallow convective moisture pump", plays an important
574 role in priming the atmosphere for increasing deep convection (e.g., [Schiro *et al.*, 2016]
575 [Zhuang *et al.*, 2017]), and wet season onset over the Amazon [Wright *et al.*, 2017].

578 The results discussed until now omitted the relation between physical processes and the
579 atmospheric composition, and more specifically the role of chemical reactions and
580 aerosol. Over rainforests, the pristine and undisturbed conditions of the atmospheric
581 boundary layer described in the seminal study by [Garstang and Fitzjarrald, 1999] are
582 currently undergoing rapid changes due to atmospheric composition modifications. Their
583 direct impact on the radiative and microphysical properties are due to biomass burning



584 and enhancement of concentrations of secondary organic aerosol precursors. Biomass
585 burning in Amazonia leads to increase aerosol optical depth and to abnormal distributions
586 of the heating rate profile. Analyzing systematic experiments performed by large-eddy
587 simulations, [Feingold *et al.*, 2005] studied the processes that lead to the suppression of
588 clouds. Firstly, at the surface there is clear indications that the latent and sensible heat
589 flux are reduced, yielding convective boundary layers characterized by less turbulent
590 intensity and by delays in the morning transition [Barbaro and Arellano, 2014]. Both
591 aspects tend to reduce cloud formations. Secondly, [Barbaro and Arellano, 2014]
592 indicated that the vertical location of the smoke layer is crucial in determining how the
593 cloud characteristics, *i.e.* cloud cover, will change. As described by [Feingold *et al.*,
594 2005], smoke confined in the well-mixed sub-cloud layer might positively benefit the
595 cloud formation since it distributes the heat uniformly that contributes to enhance
596 convection. On the other hand, smoke layers located within the cloud layer tend to
597 stabilize the cloud layer and therefore decrease the possibility of cloud formation. These
598 results are very much dependent on the aerosol optical properties defined by their
599 heating, scattering and hygroscopic properties. As a first indicative figure, the mentioned
600 LES study and observations by [Koren *et al.*, 2004] stressed that smoke layers with an
601 aerosol optical depth larger than 0.5 might already lead to cloud suppression by 50%. [Yu
602 *et al.*, 2008] have shown observationally that the influence of aerosols on shallow clouds
603 varies with meteorological conditions. When the ambient atmosphere is drier (relative
604 humidity $\leq 60\%$), the aerosol induced cloud burning effect (evaporation of cloud droplets)
605 due to increased absorption of solar radiation by aerosols out-weights the increase of cloud
606 droplets due to aerosol-cloud microphysical effect. The reduced shallow clouds can
607 further enhance the surface dryness. In contrast, when the ambient atmosphere is
608 relatively humid (relative humidity $\geq 60\%$), the aerosol-cloud microphysical effect out-
609 weighs the cloud burning effect, leading to an increase of shallow clouds and relative
610 humidity near surface. In so doing, aerosols can amplify the original moisture anomalies
611 near the surface. Aerosols have also shown to increase of the life time of mesoscale
612 convection over Congo and Amazon, due to delay of the precipitation that enhances ice
613 formation and increase lifetime of the mature and decay phase of deep convection
614 [Chakraborty *et al.*, 2016].



615 These modifications are not only related to the direct emission of aerosol, but also to
616 changes in the gas phase chemistry that act as a precursor for the formation of secondary
617 organic aerosol. [Andreae *et al.*, 2002] already described the differences in NO_x and
618 ozone (O₃) mixing ratio depending on the Amazonia site. From rather pristine conditions
619 with NO_x and ozone levels below 0.1 ppb and 20 ppb, to values above 0.1 ppb and
620 maximum levels of O₃ near 50 ppb. Recent field experiments within the Green Ocean
621 Amazon campaign (GoAmazon) (Fuentes *et al.*, 2016; [Martin *et al.*, 2016] corroborate
622 these levels as well as the high levels of the bio-organic compounds, in particular
623 isoprene and monoterpene. Closely related, these changes are accentuated by
624 anthropogenic emissions, i.e. Manaus. The unique distribution of aerosols in Amazonia
625 might explain observed differences in deep convection, in particular lightning frequency,
626 between Amazonia, the Maritime continent and the Congo basin [Williams *et al.* 2004].
627 To represent these chemistry changes and their effect on convection adequately, the
628 dynamic effect that drive processes such as the entrainment of pollutants from the free
629 troposphere need to be taken into account [Vila-Guerau de Arellano *et al.*, 2011]. As a
630 result of this interaction between radiation, the land surface, dynamics and chemical
631 processes, the transition from turbulent clear convective conditions to shallow cloudy
632 convection may be modified in the future. Current efforts in monitoring them and
633 improving the parameterizations of convection are under way [Dias *et al.*, 2014]. These
634 efforts should include also in an integrated manner the combined role of dynamics and
635 chemistry to quantify relevant processes like the ventilation of pollutants from the sub-
636 cloud layer into the cloud layer, i.e. mass flux parameterizations, under representative
637 Amazon conditions [Ouwersloot *et al.*, 2013].
638 In addition to affecting cloud microphysics, biomass burning in the tropics significantly
639 affects the global carbon budget. For example, in September and October of 2015 fires in
640 the Maritime continent released more terrestrial carbon (11.3 Tg C) than the
641 anthropogenic emissions of the EU (8.9 Tg C) [Huijnen *et al.*, 2016]. The extent of forest
642 fires in this region is tied to El Niño-induced drought conditions, and antecedent SST
643 patterns are closely related to burned area at the global scale, particularly in hotspots
644 concentrated in the tropics [Chen *et al.*, 2016]. Aerosol emissions and biomass burning
645 exert a strong control on land-atmosphere coupling of the carbon and water cycles, and
646 the consequences of this coupling is observable globally.



647 1.1. Nonlocal feedback – deep convection and large-scale circulation

648 Thus far, we have largely viewed land-atmosphere coupling through the lens of local
649 conditions, but how should we modify this view in light of remote influences (see WTG
650 discussion) or coupling between local and larger-scale conditions? Here we illustrate
651 some aspects of how land-atmosphere coupling in the Tropics is impacted by the larger-
652 scale.

653 4.1.1 Large-scale coupling, idealized modeling

654 Consider the Lagrangian tendency equation for conservation of atmospheric water
655 vapor, expressed in terms of specific humidity q :

$$656 \frac{dq}{dt} = S(q) \quad (3)$$

657 where $S(q)$ is the sum of sources and sinks of specific humidity. In the absence of
658 sources and sinks, (3) implies that the specific humidity of a parcel of air is conserved
659 following the atmospheric flow. In what follows, we consider a vertically-integrated
660 form of (3) such that:

$$661 \left\langle \frac{\partial q}{\partial t} \right\rangle = E - P - \langle \mathbf{v}_H \cdot \nabla q \rangle - \left\langle \omega \frac{\partial q}{\partial p} \right\rangle \quad (4)$$

662 Here E and P represent, respectively, the surface evapotranspiration source and the
663 precipitation sink of water vapor, while $\langle \dots \rangle$ represents a mass-weighted vertical
664 (pressure) integral from the surface (at pressure p_s) to the nominal top of the troposphere
665 (at pressure p_t), i.e., $\langle \dots \rangle = \int_{p_t}^{p_s} \dots \frac{dp}{g}$. The third and fourth terms on the right-hand side
666 (RHS) of (4) are horizontal and vertical moisture advection. Equation (4) is normalized
667 such that $\langle q \rangle$ has units of mm, thus effectively corresponding to column water vapor, and
668 terms on the right hand side are given in units of mm/day. Equation (4) is often used to
669 construct a diagnostic budget of precipitation, or in perturbation form, precipitation
670 anomalies. As a caveat, within the tropics, the dominant large-scale balance in deep
671 convecting regions is typically between vertical moisture advection (or equivalently in
672 the vertically-integrated form, moisture convergence) and precipitation, which may limit
673 the utility of (4) in attributing causality.

674 Using equation (4) as a starting point, [Lintner and Neelin, 2007; 2009] constructed a
675 framework for estimating *where* spatial transitions between tropical non-precipitating and
676 precipitating conditions, referred to as convective margins, should occur. By coupling



677 the water and energy (surface and atmosphere) equations, and invoking WTG and
678 convective quasi equilibrium assumptions, as well as a zero-surface flux constraint over
679 land, [Lintner and Neelin, 2009] derived the following expression for locating the
680 convective margin, x_c , along a prescribed inflow air-mass trajectory from an initial point
681 over the ocean onto land (see Figure 15 for a schematic overview):

$$682 \quad x_c = L_c \ln \left[\frac{q_c + q_E}{q_0 + q_E} \right] \quad (5)$$

683 L_c denotes a length scale defined as $\frac{v_q Ms}{Mq_p(R_{toa,net}-E)}$ where v_q is the mean horizontal wind
684 field, weighted with respect to the vertical moisture profile. From the WTG temperature
685 equation, and subject to the zero net surface flux constraint over land, the divergent
686 component of the large-scale circulation can be related to the net TOA radiative heating,
687 $R_{toa,net}$. Ms is the dry static stability and Mq_p the vertical moisture stratification per unit
688 moisture. The moisture values q_0 , q_c , and q_E denote, respectively, the initial inflow air
689 mass moisture, a moisture-related threshold for initiation of deep convection,; and a
690 moisture scale associated with evapotranspiration over the inflow path, $q_E = \frac{v_q E}{L_c}$. Because
691 of vertical integration, these quantities are column integrated values.

692 Note that the advantage of coupling the atmospheric moisture equation to the temperature
693 equation is that under the WTG approximation, the divergent component of the flow is
694 itself diagnosed, which can be instructive for identifying mechanisms involved. Also, in
695 equation (5) and the definition of q_E , we have assumed that $L_c > 0$ and that convergent
696 low-level flow is signed positive.

697 Evapotranspiration gives rise to two opposing effects on x_c . First, with increasing E , q_E
698 should increase, which causes x_c to decrease, i.e., moistening from evapotranspiration
699 experienced along the inflow path leads to the convective margin being reached closer to
700 the inflow point. Second, as E increases, L_c increases: this can be understood as the
701 indirect effect of E , acting through reduction of convergence along the flow path, which
702 shifts the onset point for deep convection away from the inflow point (see Figure 15).

703 Lintner et al. (2013) developed an idealized prototype for diagnosing large-scale land-
704 atmosphere coupling constructed from the idealized temperature and moisture equations
705 used in developing the convective margins model described, but further coupled to a
706 simple bucket soil moisture model. From this model, [Lintner et al., 2013] derived an



707 analytic expression for the sensitivity of precipitation to soil moisture variation from
708 which it is possible to infer dependences on key model parameters, such as the timescale
709 for convective adjustment (assumed in the Betts and Miller-type convection scheme
710 applied), cloud-radiative feedback strength, and surface turbulent flux exchange.
711 [Schaeffli *et al.*, 2012] developed a conceptually similar model from which an analytic
712 expression for the ratio of evaporated moisture integrated along flow path to precipitation
713 (or recycling ratio) was obtained (Figure 16). We suggest that such idealized model
714 frameworks, which consider tropical land-atmosphere interactions by coupling both water
715 and energy cycles, should continue to be brought to bear on observations as well as more
716 sophisticated regional or global climate or earth system models, as they can be helpful in
717 diagnosing linkages between local and non-local feedbacks.

718 4.1.2 Coupling

719 [Green *et al.*, 2017] recently developed a method to define the feedback between the
720 biosphere and atmosphere using multivariate conditional Granger causality (based on
721 lagged autoregressive vectors). We here use a similar framework using ET from
722 WECANN and precipitation from GPCP as well as photosynthetically active radiation
723 from CERES (Figure 18).

724 Most of the feedback between surface ET and precipitation occurs in the spatial
725 transitional, Monsoonal regions, such as the Savanna region of Northeastern Brazil, the
726 Monsoonal region of the Sahel and Southern Africa, as well as India and Northern
727 Australia. In Brazil, these results are consistent with the above-mentioned concept of
728 convective margin and the impact of soil moisture and transpiration rate on the location
729 of the transition between the dry and wet regions. The Sahelian and Southern African
730 Monsoon are also located in regions between very dry (deserts) and humid regions, where
731 surface feedback may be crucial for the penetration of the Monsoonal flow inland
732 [Lintner and Neelin, 2009; Lintner *et al.*, 2015]. Indeed, the biosphere in this region
733 modulates the local climate state: multiple equilibrium states, corresponding to different
734 ecosystem initial conditions, exist under the same external forcing [Wang *et al.*, 2000].
735 The effect of vegetation on land-atmosphere coupling manifests itself at multiple
736 timescales. At short timescales after precipitation, evaporation is accelerated with
737 intercepted water in the canopy. However, at longer timescales vegetation acts to delay
738 and prolong evaporation of water stored in the root zone. The magnitude and timescale of



739 these sources of water recycling will vary depending on ecosystem structure, including
740 rooting depth and canopy structure, which may co-evolve with atmospheric conditions at
741 the interannual timescale [Nicholson, 2000]. This represents a clear pathway for two-way
742 feedbacks between the land surface and precipitation.

743 We further emphasize that those feedbacks (Figure 18) are likely to also be influenced by
744 non-local conditions, with regional and large-scale changes in ocean to land flow and the
745 in-land distance of penetration influencing local coupling. We note that climate models
746 seem to exhibit soil moisture (and therefore evapotranspiration)- precipitation feedbacks
747 in similar tropical regions, when averaged across models, even though individual model
748 response varies [Koster *et al.*, 2011; Seneviratne, 2013] (one degree pixel and monthly
749 time scales). We emphasize that the PAR radiation product is very uncertain in the
750 tropics [Jimenez *et al.*, 2011] as it ultimately relies on a model to obtain surface incoming
751 radiation, which might explain the reduced feedback strength. It is also likely that the
752 bulk of the radiative feedbacks are taking place at smaller times scales such as the ones
753 observed with MODIS (Figure 14). This shallow cloud cover is relatively steady spatially
754 and in time, especially in the dry season.

755 4.1.3 Moisture tracking and source attribution

756 A fundamental consideration in the study of the hydrologic cycle over tropical
757 continents is where the moisture for precipitation ultimately derives. As [van der Ent *et*
758 *al.*, 2010; van der Ent and Tuinenburg, 2017] note, this consideration is not merely of
759 academic interest: indeed, it is quite likely that anthropogenic modification of the land
760 surface has altered terrestrial evapotranspiration (as well as runoff) to impact
761 precipitation. A common approach to moisture source attribution over tropical land
762 regions involves deriving air mass histories using Lagrangian trajectories. Such
763 trajectories are obtained by temporally integrating the 3-dimensional wind field to
764 estimate the positions of idealized air mass parcels through time. Trajectories can be
765 computed in either a forward or backward sense: the latter are initialized from an arrival
766 point and integrated backward through time. Combining a Lagrangian back trajectory
767 approach with rainfall and leaf area index data, [Spracklen *et al.*, 2012] quantified the
768 linkage between downstream rainfall amount and upstream air mass exposure to
769 vegetation (Figure 17). Over more than half of the tropical land surface, the Spracklen
770 *et al.* estimates indicate a twofold increase in downstream rainfall for those air masses



771 passing over extensive vegetation compared those passing over little upstream vegetation.
772 Based on these estimates and extrapolating current Amazonian deforestation trends in the
773 future, these authors project wet and dry season rainfall decreases of 12 and 21%,
774 respectively, by the year 2050.

775 Other analyses using air mass histories have demonstrated the significance of terrestrial *E*
776 sources for remote land regions. For example, [Drumond *et al.*, 2014] used the
777 FLEXPART model forced with ERA-Interim reanalysis to estimate *E* – *P* along
778 trajectories passing over the La Plata Basin in subtropical South America to establish that
779 much of the moisture entering this region derives from the Amazon Basin to the north
780 and west.

781

782 4.1.4 Seasonality and seasonal transitions

783 One of the outstanding issues in the study of tropical land region climates involves
784 controls on precipitation seasonality, particularly its regional variability. To leading
785 order, the seasonality follows the variation in maximum solar heating, but other factors,
786 such as ocean thermal inertia, topography, dynamics and circulation, and moisture
787 transport, as well as the state of the land surface, can exert considerable influence on the
788 timing and amplitude of tropical land region seasonal evolution. Over the Amazon basin,
789 seasonality exhibits marked variation in both latitude and longitude: for example, at 5S,
790 the dry-to-west transition proceeds from the central Amazon eastward toward the Atlantic
791 coast [Liebmann and Marengo, 2001]. It is also worth noting a pervasive tendency for
792 the dry-to-wet season transition to occur much more rapidly than the wet-to-dry
793 transition, as evident in tropical monsoon systems including South Asia, West Africa, and
794 South America.

795 Analyzing multiple observational and reanalysis products, [Fu and Li, 2004]
796 identified a strong influence of surface turbulent fluxes on the dry-to-wet transition and
797 its interannual variability over the Amazon. In particular, their results link earlier wet
798 season onset to wetter conditions in the antecedent dry season: the higher latent fluxes at
799 the end of a wetter dry season encourage weaker convective inhibition (CIN) but
800 enhanced CAPE, both of which are more favorable to wet season rainfall occurrence.
801 However, these authors also underscore the participation of the large-scale circulation
802 and its role in establishing a background environment (e.g., moisture convergence) to



803 support wet season rainfall. Incursion of cold fronts into the southern Amazon may act as
804 triggers for rapid initiation of wet season onset once the local thermodynamics become
805 favorable [*Li et al.*, 2006].

806 Recent researches suggest that the land-atmospheric coupling plays a central role in
807 determining the earlier timing of the wet season onset over western and southern
808 Amazonia, relative to that of eastern Amazonia. Both in situ and satellite ecological
809 observations have consistently shown that rainforests increase their photosynthesis, thus
810 evapotranspiration (ET), during late dry season across Amazonia (e.g., [*Huete et al.*,
811 2006; *Lopes et al.*, 2016; *Munger et al.*, 2016; *Wehr et al.*, 2016]). The wet season onset
812 over the southern hemispheric western and southern Amazonia occurs during September
813 to October, about two to three months before the arrival of the Atlantic ITCZ [*Fu et al.*,
814 2016]. Using several satellite measurements, including deuterium (HDO) of the
815 atmospheric water vapor and SIF, Wright et al (2017) have shown that such an increase
816 of ET in the late dry season is the primary source of increasing water vapor in the lower
817 troposphere that initiates the increase of deep convection and rainfall over southern
818 Amazonia. In particular, the increase of water vapor with enriched HDO in the boundary
819 layer and free troposphere, follows the increase of photosynthesis during late dry season.
820 The HDO value of the atmospheric moisture is too high to be explained by transport from
821 Atlantic Ocean, and is consistent with that from plant transpiration. Such a moistening of
822 the atmosphere starts in western southern Amazonia, the part of Amazonia that is most
823 remote from the Atlantic Ocean with high biomass. It then progresses towards eastern
824 southern Amazonia. Thus, during the late dry season this appears to contribute to the
825 timing and spatial variation of the initial moistening of the atmosphere, that ultimately
826 lead to wet season onset over southern Amazonia.

827 Wet season onset over southern Amazonia has been delaying since the late 1970s
828 [*Marengo et al.*, 2011; *Fu et al.*, 2013]. In addition to the influence of global circulation
829 change, such a change has been attributed to land use. For example, [*Butt et al.*, 2011]
830 have compared long-term rainfall data between deforested and forested areas over part of
831 the southern Amazonia. They observed a significant delay in wet season onset over the
832 deforested areas, consistent with that implied by Wright et al. (2017). In addition, [*Zhang*
833 *et al.*, 2008; 2009] have shown that biomass burning aerosols, which peak in late dry



834 season, can also weaken and delay dry to wet season transition by stabilizing the
835 atmosphere, reducing clouds and rainfall.

836 5 Discussion - conclusions

837 In this review paper, we have discussed some of the important aspects of land-
838 atmosphere interactions pertaining to the tropics. This review article is by no means
839 exhaustive but rather provides insights into some of the important coupled land-
840 atmosphere processes at play in the tropics and in rainforest ecosystems in particular.

841 We have argued that feedbacks between the land surface and precipitation in the tropics
842 are possibly non-local in nature and mostly impact moisture advection from the ocean
843 and the position of deep convection onset. Local rainfall feedback associated with
844 mesoscale heterogeneities appear to be rather small in magnitude, at least compared to
845 the annual-mean rainfall, and not sufficiently spatially systematic to truly affect
846 ecosystem functioning.

847 Moreover, we contend that land surface-cloud feedbacks, especially those involving
848 shallow clouds and fog, are critical in terms of regulating light (direct and diffuse),
849 temperature, and water vapor deficit over tropical forest, but such feedbacks have
850 received relatively little attention. Remote sensing platforms provide useful information
851 for quantifying such feedbacks, but these need to be complemented by ground
852 measurements (especially of photosynthetic rates and respiration). Eddy-covariance
853 measurements may prove difficult to use, as mesoscale circulations alter the homogeneity
854 assumption of eddy-covariance methods.

855 We have also discussed errors and biases in the representation of tropical continental
856 climates in current generation climate and Earth system models. The average soil
857 moisture-precipitation feedback strength across earth system models (based on the
858 GLACE experiment) [Koster *et al.*, 2004] tend to exhibit land-precipitation feedbacks in
859 similar transitional regions as the ones observed, which seems to be mostly related to
860 modification of the moisture advection penetration distance from the ocean rather than to
861 local feedbacks. These feedbacks appear to be of relatively minor importance in the core
862 of tropical rainforests but are more critical for more marginal rainfall regions (savanna).
863 These regions are of critical importance for the terrestrial global carbon cycle, providing
864 the main terrestrial sink, but might be severely impacted by climate change and droughts



865 in particular [*Laan Luijkx et al.*, 2015]. Whether the interannual variability in surface CO₂
866 flux in those regions is a zero-sum game with wet years compensating dry years still is an
867 open question especially in the context of rising CO₂ concentration.

868 The core of rainforests seems to be more affected by radiation feedbacks at relatively
869 small spatial scales (~1km), which can be dramatically influenced by land cover and land
870 use change. Projected rates of future deforestation are poorly constrained, especially
871 regionally, though in recent years, the Congo and Indonesia have experienced increasing
872 deforestation while the deforestation rate in the Amazon has dropped.

873 Earth system models tend to predict very diverse responses to global warming leading to
874 broad spread in the capacity of rainforests to continue to act as net carbon sinks [*Swann et*
875 *al.*, 2015] in the future. Indeed, in the Amazon in particular, the models' response varies
876 from becoming much drier to more humid. El Niño events are sometimes thought as a
877 proxy of global warming in the tropics [*Pradipta et al.*, 2016] as they warm the free-
878 troposphere. Nonetheless for continents the change in the Walker circulation associated
879 with El Niño may strongly differ from the change associated with a more uniform sea
880 surface temperature warming in future climate. In particular, mature El Niño events are
881 associated with strong subsidence over Indonesia, increased ascent off the coast of Peru
882 but reduced precipitation over the Amazon basin and a relatively neutral response over
883 the Congo basin. With SST warming across the tropics, the Maritime continent will most
884 likely become wetter [*Byrne and O'Gorman*, 2015; *Wills et al.*, 2016]. The fate of the
885 Amazon basin is less clear, as the climate in the region will be impacted by a
886 combination of free tropospheric warming stabilizing the atmosphere to deep convection
887 while warming of the Atlantic enhances the low-level MSE of inflow into the basin.
888 Additionally, warming-induced changes to large-scale circulation such as the intensity or
889 orientation of low-level Atlantic trade winds could impact Amazonian precipitation
890 change. Knowledge of the Congo basin remains limited but it appears that the basin will
891 become dryer under the combined effect of increased temperature and reduced
892 precipitation [*Greve et al.*, 2014]. One important question involves how the effect of
893 rising [CO₂] modifies surface energy flux partitioning though changes in stomatal
894 physiology and modify the regional climate though land-atmosphere interactions
895 [*Lemordant*, 2016].

896



897 *Acknowledgments.* This work was supported by Pierre Gentine’s new investigator
898 grant NNX14AI36G, DOE Early Career grant DE-SC0014203, NSF CAREER and
899 GoAmazon DE-SC0011094. We would like to acknowledge high-performance computing
900 support from Yellowstone (<ark:/85065/d7wd3xhc>) provided by NCAR's Computational
901 and Information Systems Laboratory, sponsored by the National Science Foundation.
902



903 REFERENCES

904

905 Acevedo, O. C., O. L. L. Moraes, R. da Silva, D. R. Fitzjarrald, R. K. Sakai, R. M.
906 Staebler, and M. J. Czikowsky, Inferring nocturnal surface fluxes from vertical
907 profiles of scalars in an Amazon pasture, *Global Change Biol*, 10(5), 886–894,
908 doi:10.1111/j.1529-8817.2003.00755.x, 2004.

909 Alemohammad, S. H., B. Fang, A. G. Konings, F. Aires, J. K. Green, J. Kolassa, D.
910 Miralles, C. Prigent, and P. Gentine, Water, Energy, and Carbon with Artificial
911 Neural Networks (WECANN): a statistically based estimate of global surface
912 turbulent fluxes and gross primary productivity using solar-induced fluorescence,
913 *Biogeosciences*, 14(18), 4101–4124, doi:10.5194/bg-14-4101-2017, 2017.

914 Alemohammad, S. H., B. Fang, A. G. Konings, J. K. Green, J. Kolassa, C. Prigent, F.
915 Aires, D. Miralles, and P. Gentine, Water, Energy, and Carbon with Artificial Neural
916 Networks (WECANN): A statistically-based estimate of global surface turbulent
917 fluxes using solar-induced fluorescence,, 1–36, doi:10.5194/bg-2016-495, 2016.

918 Alexander, J. N., J. R. Peter, and N. K. Ernest, Assimilating solar-induced chlorophyll
919 fluorescence into the terrestrial biosphere model BETHY-SCOPE: Model description
920 and information content, *geosci-model-dev-discuss.net*, doi:10.5194/gmd-2017-34,
921 2017.

922 Anber, U., P. Gentine, S. Wang, and A. H. Sobel, Fog and rain in the Amazon,
923 *Proceedings of the National Academy of Sciences*, 112(37), 11473–11477,
924 doi:10.1073/pnas.1505077112, 2015.

925 Anber, U., S. Wang, and A. Sobel, Effect of Surface Fluxes versus Radiative Heating on
926 Tropical Deep Convection, *Journal of Atmospheric Sciences*, 72(9), 3378–3388,
927 doi:10.1175/JAS-D-14-0253.1, 2015.

928 Andreae, M.O., Artaxo, P., Brandao, C., Carswell, F.E., Ciccioli, P., Da Costa, A.L.,
929 Culf, A.D., Esteves, J.L., Gash, J.H.C., Grace, J. and Kabat, P., Biogeochemical
930 cycling of carbon, water, energy, trace gases, and aerosols in Amazonia: The LBA-



- 931 EUSTACH experiments, *J Geophys Res-Atmos*, 107(D20),
932 doi:10.1029/2001JD000524, 2002.
- 933 Andreasen, M., K. H. Jensen, D. Desilets, M. Zreda, H. Bogen, and M. C. Looms, Can
934 canopy interception and biomass be inferred from cosmic-ray neutron intensity?
935 Results from neutron transport modeling,, 1–42, doi:10.5194/hess-2016-226, 2016
- 936 Avissar, R., and C. Nobre, Preface to special issue on the Large-Scale Biosphere-
937 Atmosphere Experiment in Amazonia (LBA), *J Geophys Res-Atmos*, 107, –,
938 doi:10.1029/2002JD002507, 2002
- 939 Avissar, R., and R. A. Pielke, A parameterization of heterogeneous land surfaces for
940 atmospheric numerical models and its impact on regional meteorology, *Mon Wea*
941 *Rev.*, 1989.
- 942 Avissar, R., and T. Schmidt, An evaluation of the scale at which ground-surface heat flux
943 patchiness affects the convective boundary layer using large-eddy simulations, *J*
944 *Atmos Sci*, 55(16), 2666–2689, 1998.
- 945 Avissar, R., P. Dias, M. Dias, and C. Nobre, The Large-Scale Biosphere-atmosphere
946 Experiment in Amazonia (LBA): Insights and future research needs, *J Geophys Res-*
947 *Atmos*, 107(D20), doi:10.1029/2002JD002704, 2002.
- 948 Baldocchi, D., Falge, E., Gu, L., Olson, R., Hollinger, D., Running, S., Anthoni, P.,
949 Bernhofer, C., Davis, K., Evans, R. and Fuentes, J., FLUXNET: A new tool to study
950 the temporal and spatial variability of ecosystem-scale carbon dioxide, water vapor,
951 and energy flux densities, *Bull. Amer. Meteor. Soc.*, 82(11), 2415–2434, 2001.
- 952 Ballantyne, A., Smith, W., Anderegg, W., Kauppi, P., Sarmiento, J., Tans, P.,
953 Shevliakova, E., Pan, Y., Poulter, B., Anav, A. and Friedlingstein, P., Accelerating
954 net terrestrial carbon uptake during the warming hiatus due to reduced respiration,
955 *Nature Climate Change*, 7(2), 148–152, doi:10.1038/nclimate3204, 2017.
- 956 Balsamo, G., A. Beljaars, K. Scipal, P. Viterbo, B. van den Hurk, M. Hirschi, and A. K.
957 Betts, A Revised Hydrology for the ECMWF Model: Verification from Field Site to



- 958 Terrestrial Water Storage and Impact in the Integrated Forecast System, *J*
959 *Hydrometeorol*, 10(3), 623–643, doi:10.1175/2008JHM1068.1, 2009.
- 960 Barbaro, E., and J. Arellano, Aerosols in the convective boundary layer: Shortwave
961 radiation effects on the coupled land-atmosphere system , *J of Climate*,
962 doi:10.1002/(ISSN)2169-8996., 2014
- 963 Bechtold, P., N. Semane, P. Lopez, J.-P. Chaboureau, A. Beljaars, and N. Bormann,
964 Representing equilibrium and non-equilibrium convection in large-scale models, *J*
965 *Atmos Sci*, 71(2), 130919100122007–753, doi:10.1175/JAS-D-13-0163.1, 2013.
- 966 Bechtold, P., N. Semane, P. Lopez, J.-P. Chaboureau, A. Beljaars, and N. Bormann,
967 Representing Equilibrium and Nonequilibrium Convection in Large-Scale Models, *J*
968 *Atmos Sci*, 71(2), 734–753, doi:10.1175/JAS-D-13-0163.1, 2014.
- 969 Betts, A. K., and M. A. F. Silva Dias, Progress in understanding land-surface-atmosphere
970 coupling from LBA research, *J. Adv. Model. Earth Syst.*, 2, 6,
971 doi:10.3894/JAMES.2010.2.6, 2010.
- 972 Betts, A. K., L. V. Gatti, and A. M. Cordova, Transport of ozone to the surface by
973 convective downdrafts at night, *J of Climate*, 2002.
- 974 Boisier, J. P., P. Ciais, A. Ducharne, and M. Guimberteau, Projected strengthening of
975 Amazonian dry season by constrained climate model simulations, *Nature Climate*
976 *Change*, 5(7), 656–660, doi:10.1038/nclimate2658, 2015.
- 977 Bonan, G. B., K. W. Oleson, and R. A. Fisher, Reconciling leaf physiological traits and
978 canopy flux data: Use of the TRY and FLUXNET databases in the Community Land
979 Model version 4 , *J of Climate*, 2012.
- 980 Bonan, G. B., P. J. Lawrence, K. W. Oleson, S. Levis, M. Jung, M. Reichstein, D. M.
981 Lawrence, and S. C. Swenson, Improving canopy processes in the Community Land
982 Model version 4 (CLM4) using global flux fields empirically inferred from
983 FLUXNET data, *J Geophys Res-Biogeo*, 116, 1–22, doi:10.1029/2010JG001593,
984 2011.



- 985 Boone, A., De Rosnay, P., Balsamo, G., Beljaars, A., Chopin, F., Decharme, B., Delire,
986 C., Ducharne, A., Gascoin, S., Grippa, M. and Guichard, F., The AMMA Land
987 Surface Model Intercomparison Project (ALMIP), *Bull. Amer. Meteor. Soc.*, 90(12),
988 1865–1880, doi:10.1175/2009BAMS2786.1, 2009.
- 989 Boone, A., A. Getirana, J. Demarty, and B. Cappelaere, The African Monsoon
990 Multidisciplinary Analyses (AMMA) Land surface Model Intercomparison Project
991 Phase 2 (ALMIP2), *GEWEX News*, 2009
- 992 Boulet, G., A. Chehbouni, P. Gentine, B. Duchemin, J. Ezzahar, and R. Hadria,
993 Monitoring water stress using time series of observed to unstressed surface
994 temperature difference, *Agr Forest Meteorol*, 146, 159–172,
995 doi:10.1016/j.agrformet.2007.05.012, 2007.
- 996 Böing, S. J., H. J. J. Jonker, A. P. Siebesma, and W. W. Grabowski, Influence of the
997 Subcloud Layer on the Development of a Deep Convective Ensemble, *J Atmos Sci*,
998 69(9), 2682–2698, doi:10.1175/JAS-D-11-0317.1, 2012.
- 999 Bretherton, C. S., and S. Park, A New Moist Turbulence Parameterization in the
1000 Community Atmosphere Model, *J Climate*, 22(12), 3422–3448,
1001 doi:10.1175/2008JCLI2556.1, 2009.
- 1002 Brodribb, T. J. Stomatal Closure during Leaf Dehydration, Correlation with Other Leaf
1003 Physiological Traits, *Plant Physiol*, 132(4), 2166–2173, doi:10.1104/pp.103.023879,
1004 2003.
- 1005 Butt, N., P. A. de Oliveira, and M. H. Costa, Evidence that deforestation affects the onset
1006 of the rainy season in Rondonia, Brazil, *Journal of Geophysical Research:*
1007 *Atmospheres (1984–2012)*, 116(D11), 407, doi:10.1029/2010JD015174, 2011.
- 1008 Byrne, M. P., and P. A. O’Gorman, The Response of Precipitation Minus
1009 Evapotranspiration to Climate Warming: Why the “Wet-Get-Wetter, Dry-Get-
1010 Drier” Scaling Does Not Hold over Land, *J Climate*, doi:10.1175/JCLI-D-15-
1011 0369.s1, 2015.



- 1012 Campos, J. G., O. C. Acevedo, J. Tota, and A. O. Manzi, On the temporal scale of the
1013 turbulent exchange of carbon dioxide and energy above a tropical rain forest in
1014 Amazonia, *J Geophys Res*, *114*(D8), D08124–10, doi:10.1029/2008JD011240., 2009
- 1015 Canal, N., J. C. Calvet, B. Decharme, D. Carrer, S. Lafont, and G. Pigeon, Evaluation of
1016 root water uptake in the ISBA-A-gs land surface model using agricultural yield
1017 statistics over France, *Hydrol Earth Syst Sc*, *18*(12), 4979–4999, doi:10.5194/hess-
1018 18-4979-2014-supplement, 2014.
- 1019 Chagnon, F. J. F., R. L. Bras, and J. Wang, Climatic shift in patterns of shallow clouds
1020 over the Amazon, *Geophys Res Lett*, *31*(24), L24212, doi:10.1029/2004GL021188,
1021 2004.
- 1022 Chaney, N. W., J. D. Herman, M. B. Ek, and E. F. Wood, Deriving Global Parameter
1023 Estimates for the Noah Land Surface Model using FLUXNET and Machine
1024 Learning, *J Geophys Res-Atmos*, 1–41, doi:10.1002/2016JD024821, 2016.
- 1025 Chen, Y., Ryder, J., Bastrikov, V., McGrath, M.J., Naudts, K., Otto, J., Ottlé, C., Peylin,
1026 P., Polcher, J., Valade, A. and Black, A., Evaluating the performance of land surface
1027 model ORCHIDEE-CAN v1.0 on water and energy flux estimation with a single- and
1028 multi-layer energy budget scheme, *Geosci Model Dev*, *9*(9), 2951–2972,
1029 doi:10.5194/gmd-9-2951-2016, 2016.
- 1030 Chor, T. L., N. L. Dias, A. Araújo, S. Wolff, E. Zahn, A. Manzi, I. Trebs, M. O. Sá, P. R.
1031 Teixeira, and M. Sörgel, Flux-variance and flux-gradient relationships in the
1032 roughness sublayer over the Amazon forest, *Agr Forest Meteorol*, *239*, 213–222,
1033 doi:10.1016/j.agrformet.2017.03.009, 2017.
- 1034 Cook, B. I., S. P. Shukla, M. J. Puma, and L. S. Nazarenko, Irrigation as an historical
1035 climate forcing, *Climate dynamics*, *44*(5-6), 1715–1730, doi:10.1007/s00382-014-
1036 2204-7, 2014.
- 1037 Couvreux, F., Roehrig, R., Rio, C., Lefebvre, M.P., Caian, M., Komori, T., Derbyshire,
1038 S., Guichard, F., Favot, F., D'Andrea, F. and Bechtold, P., Representation of daytime
1039 moist convection over the semi-arid Tropics by parametrizations used in climate and



- 1040 meteorological models, *Q J Roy Meteor Soc*, 141(691), 2220–2236,
1041 doi:10.1002/qj.2517, 2015.
- 1042 Couvreur, F., C. Rio, and F. Guichard, Initiation of daytime local convection in a semi-
1043 arid region analysed with high-resolution simulations and AMMA observations -
1044 Quarterly Journal of the Royal Meteorological Society, 2011
- 1045 Couvreur, F., C. Rio, F. Guichard, M. Lothon, G. Canut, D. Bouniol, and A. Gounou,
1046 Initiation of daytime local convection in a semi-arid region analysed with high-
1047 resolution simulations and AMMA observations, *Q J Roy Meteor Soc*, 138(662), 56–
1048 71, doi:10.1002/qj.903, 2011.
- 1049 Da Rocha, H. R. et al., Patterns of water and heat flux across a biome gradient from
1050 tropical forest to savanna in Brazil, *J Geophys Res*, 114, G00B12,
1051 doi:10.1029/2007JG000640, 2009.
- 1052 Daleu, C. L., S. J. Woolnough, and R. S. Plant (2012), Cloud-Resolving Model
1053 Simulations with One- and Two-Way Couplings via the Weak Temperature Gradient
1054 Approximation, *J Atmos Sci*, 69(12), 3683–3699, doi:10.1175/JAS-D-12-058.1.
- 1055 Daleu, C. L., S. J. Woolnough, and R. S. Plant, Transition from suppressed to active
1056 convection modulated by a weak-temperature gradient derived large-scale
1057 circulation, *J Atmos Sci*, 141023140130007, doi:10.1175/JAS-D-14-0041.1, 2014.
- 1058 Dalu, G. A., R. A. Pielke, M. Baldi, and X. Zeng, Heat and momentum fluxes induced by
1059 thermal inhomogeneities with and without large-scale flow, *Journal of the*
1060 *atmospheric Science*, 1996.
- 1061 Davidson, E.A., de Araújo, A.C., Artaxo, P., Balch, J.K., Brown, I.F., Bustamante, M.M.,
1062 Coe, M.T., DeFries, R.S., Keller, M., Longo, M. and Munger, J.W., The Amazon
1063 basin in transition, *Nature*, 481(7381), 321–328, doi:10.1038/nature10717, 2012
- 1064 de Arellano, J. V.-G., H. G. Ouwersloot, D. Baldocchi, and C. M. J. Jacobs, Shallow
1065 cumulus rooted in photosynthesis, *Geophys Res Lett*, doi:10.1002/2014GL059279,
1066 2014.



- 1067 De Kauwe, M. G., J. Kala, Y. S. Lin, A. J. Pitman, B. E. Medlyn, R. A. Duursma, G.
1068 Abramowitz, Y. P. Wang, and D. G. Miralles, A test of an optimal stomatal
1069 conductance scheme within the CABLE land surface model, *Geosci Model Dev*, 8(2),
1070 431–452, doi:10.5194/gmd-8-431-2015, 2015.
- 1071 Del Genio, A. D., and J. Wu, The Role of Entrainment in the Diurnal Cycle of
1072 Continental Convection, *J Climate*, 23(10), 2722–2738,
1073 doi:10.1175/2009JCLI3340.1, 2010.
- 1074 Domec, J.-C., J. S. King, A. Noormets, E. Treasure, M. J. Gavazzi, G. Sun, and S. G.
1075 McNulty, Hydraulic redistribution of soil water by roots affects whole-stand
1076 evapotranspiration and net ecosystem carbon exchange, *New Phytologist*, 187(1),
1077 171–183, doi:10.1111/j.1469-8137.2010.03245.x, 2010.
- 1078 Doughty, C.E., Metcalfe, D.B., Girardin, C.A.J., Amézquita, F.F., Cabrera, D.G., Huasco,
1079 W.H., Silva-Espejo, J.E., Araujo-Murakami, A., Da Costa, M.C., Rocha, W. and
1080 Feldpausch, T.R., Drought impact on forest carbon dynamics and fluxes in
1081 Amazonia, *Nature*, 519(7541), 78–82, doi:10.1038/nature14213, 2015.
- 1082 Drager, A. J., and S. C. van den Heever, Characterizing convective cold pools, *J. Adv.*
1083 *Model. Earth Syst.*, 1–55, doi:10.1002/2016MS000788, 2017.
- 1084 Drumond, A., J. Marengo, T. Ambrizzi, R. Nieto, L. Moreira, and L. Gimeno, The role of
1085 the Amazon Basin moisture in the atmospheric branch of the hydrological cycle: a
1086 Lagrangian analysis, *Hydrol Earth Syst Sc*, 18(7), 2577–2598, doi:10.5194/hess-18-
1087 2577-2014, 2014.
- 1088 Du, S., L. Liu, X. Liu, and J. Hu, Response of Canopy Solar-Induced Chlorophyll
1089 Fluorescence to the Absorbed Photosynthetically Active Radiation Absorbed by
1090 Chlorophyll, *Remote Sensing*, 9(9), 911–19, doi:10.3390/rs9090911, 2017.
- 1091 Duveiller, G., and A. Cescatti, Spatially downscaling sun-induced chlorophyll
1092 fluorescence leads to an improved temporal correlation with gross primary
1093 productivity, *Remote Sensing of Environment*, 182(C), 72–89,
1094 doi:10.1016/j.rse.2016.04.027, 2016.



- 1095 D'Andrea, F., P. Gentine, and A. K. Betts, Triggering deep convection with a
1096 probabilistic plume model, *J Atmos Sci*, 71(11), 3881–3901, doi:10.1175/JAS-D-13-
1097 0340.1, 2014.
- 1098 Ek, M. B., Implementation of Noah land surface model advances in the National Centers
1099 for Environmental Prediction operational mesoscale Eta model, *J Geophys Res*,
1100 108(D22), 8851, doi:10.1029/2002JD003296, 2003.
- 1101 Engerer, N. A., D. J. Stensrud, and M. C. Coniglio, Surface Characteristics of Observed
1102 Cold Pools, *Mon Wea Rev*, 136(12), 4839–4849, doi:10.1175/2008MWR2528.1,
1103 2008.
- 1104 Feingold, G., H. L. Jiang, and J. Y. Harrington, On smoke suppression of clouds in
1105 Amazonia, *Geophys Res Lett*, 32(2), doi:10.1029/2004GL021369, 2005.
- 1106 Feng, Z., S. Hagos, A. K. Rowe, C. D. Burleyson, M. N. Martini, and S. P. de Szoeke,
1107 Mechanisms of convective cloud organization by cold pools over tropical warm
1108 ocean during the AMIE/DYNAMO field campaign, *J. Adv. Model. Earth Syst.*, 7(2),
1109 357–381, doi:10.1002/2014MS000384, 2015.
- 1110 Fisher, J.B., Malhi, Y., Bonal, D., Da Rocha, H.R., De Araujo, A.C., Gamo, M., Goulden,
1111 M.L., Hirano, T., Huete, A.R., Kondo, H. and Kumagai, T.O., The land-atmosphere
1112 water flux in the tropics, *Global Change Biol*, 15(11), 2694–2714,
1113 doi:10.1111/j.1365-2486.2008.01813.x, 2009.
- 1114 Fisher, R. A., M. Williams, R. L. Do Vale, A. L. Da Costa, and P. Meir, Evidence from
1115 Amazonian forests is consistent with isohydric control of leaf water potential, *Plant*
1116 *Cell Environ*, 29(2), 151–165, 2006.
- 1117 Fitzjarrald, D. R., Turbulent transport just above the Amazon, *J Geophys Res-Atmos*, 1–
1118 13, 2007.
- 1119 Frankenberg, C., Fisher, J.B., Worden, J., Badgley, G., Saatchi, S.S., Lee, J.E., Toon,
1120 G.C., Butz, A., Jung, M., Kuze, A. and Yokota, T., New global observations of the
1121 terrestrial carbon cycle from GOSAT: Patterns of plant fluorescence with gross



- 1122 primary productivity, *Geophys Res Lett*, 38(17), n/a–n/a,
1123 doi:10.1029/2011GL048738, 2011.
- 1124 Frankenberg, C., C. O'Dell, J. Berry, L. Guanter, J. Joiner, P. Köhler, R. Pollock, and T.
1125 E. Taylor, Prospects for chlorophyll fluorescence remote sensing from the Orbiting
1126 Carbon Observatory-2, *Remote Sensing of Environment*, 147(C), 1–12,
1127 doi:10.1016/j.rse.2014.02.007, 2014.
- 1128 Frankenberg, C., C. O'Dell, L. Guanter, and J. McDuffie, Remote sensing of near-
1129 infrared chlorophyll fluorescence from space in scattering atmospheres: implications
1130 for its retrieval and interferences with atmospheric CO₂ retrievals, *Atmos Meas Tech*,
1131 5(8), 2081–2094, doi:10.5194/amt-5-2081-2012, 2012.
- 1132 Fu, R., and W. Li, The influence of the land surface on the transition from dry to wet
1133 season in Amazonia, *Theor Appl Climatol*, 78(1-3), 97–110, doi:10.1007/s00704-
1134 004-0046-7., 2004
- 1135 Fu, R., L. Yin, W. Li, and P. A. Arias, Increased dry-season length over southern
1136 Amazonia in recent decades and its implication for future climate projection, 2013.
- 1137 Fu, R., P. A. Arias, and H. Wang, The Connection Between the North and South
1138 American Monsoons, *The Monsoons and Climate Change*, 2016
- 1139 Garstang, M., and D. R. Fitzjarrald, *Observations of surface to atmosphere interactions*
1140 *in the tropics.*, 1999
- 1141 Gatti, L.V., Gloor, M., Miller, J.B., Doughty, C.E., Malhi, Y., Domingues, L.G., Basso,
1142 L.S., Martinewski, A., Correia, C.S.C., Borges, V.F. and Freitas, S., Drought
1143 sensitivity of Amazonian carbon balance revealed by atmospheric measurements,
1144 *Nature*, 506(7486), 76–80, doi:10.1038/nature12957, 2015.
- 1145 Gentine, P., A. Garelli, S. B. Park, and J. Nie, Role of surface heat fluxes underneath cold
1146 pools, *Geo Res Letters*, 43(2), 874–883, doi:10.1002/2015GL067262, 2016.



- 1147 Gentine, P., A. Holtslag, and F. D'Andrea, Surface and atmospheric controls on the onset
1148 of moist convection over land, *J Hydrometeorol*, 14(5), 1443–1462,
1149 doi:10.1175/JHM-D-12-0137.1, 2013.
- 1150 Gentine, P., C. R. Ferguson, and A. A. M. Holtslag, Diagnosing evaporative fraction over
1151 land from boundary-layer clouds, *J Geophys Res-Atmos*, 118(15), 8185–8196,
1152 doi:10.1002/jgrd.50416, 2013.
- 1153 Gentine, P., D. Entekhabi, A. Chehbouni, G. Boulet, and B. Duchemin, Analysis of
1154 evaporative fraction diurnal behaviour, *Agr Forest Meteorol*, 143, 13–29,
1155 doi:10.1016/j.agrformet.2006.11.002, 2007.
- 1156 Gerken, T., Ruddell, B.L., Fuentes, J.D., Araújo, A., Brunsell, N.A., Maia, J., Manzi, A.,
1157 Mercer, J., dos Santos, R.N., von Randow, C. and Stoy, P.C., Investigating the
1158 mechanisms responsible for the lack of surface energy balance closure in a central
1159 Amazonian tropical rainforest, *Agr Forest Meteorol*, 1–0,
1160 doi:10.1016/j.agrformet.2017.03.023, 2017.
- 1161 Ghate, V. P., and P. Kollias, On the controls of daytime precipitation in the Amazonian
1162 dry season, *J Hydrometeorol*, JHM–D–16–0101.1–55, doi:10.1175/JHM-D-16-
1163 0101.1, 2016.
- 1164 Giangrande, S. E. et al., Cloud Characteristics, Thermodynamic Controls and Radiative
1165 Impacts During the Observations and Modeling of the Green Ocean Amazon
1166 (GoAmazon2014/5) Experiment, *Atmos. Chem. Phys. Discuss.*, 1–41,
1167 doi:10.5194/acp-2017-452, 2017.
- 1168 Goulden, M. L., S. D. Miller, and H. R. da Rocha, Diel and seasonal patterns of tropical
1169 forest CO₂ exchange, *Ecological*, 2004
- 1170 Green, J. K., A. G. Konings, S. H. Alemohammad, J. Berry, D. Entekhabi, J. Kolassa, J.-
1171 E. Lee, and P. Gentine, Regionally strong feedbacks between the atmosphere and
1172 terrestrial biosphere, *Nat Geosci*, 48, 1–12, doi:10.1038/ngeo2957, 2017.



- 1173 Greve, P., B. Orlowsky, B. Mueller, J. Sheffield, M. Reichstein, and S. I. Seneviratne,
1174 Global assessment of trends in wetting and drying over land, *Nat Geosci*, 7(10), 716–
1175 721, doi:10.1038/ngeo2247, 2014.
- 1176 Guanter, L., Zhang, Y., Jung, M., Joiner, J., Voigt, M., Berry, J.A., Frankenberg, C.,
1177 Huete, A.R., Zarco-Tejada, P., Lee, J.E. and Moran, Global and time-resolved
1178 monitoring of crop photosynthesis with chlorophyll fluorescence, *PNAS*, 111(14),
1179 E1327–E1333, doi:10.1073/pnas.1320008111, 2014.
- 1180 Guichard, F., Petch, J.C., Redelsperger, J.L., Bechtold, P., Chaboureaud, J.P., Cheinet, S.,
1181 Grabowski, W., Grenier, H., Jones, C.G., Köhler, M. and Piriou, J.M., Modelling the
1182 diurnal cycle of deep precipitating convection over land with cloud-resolving models
1183 and single-column models, *Q J Roy Meteor Soc*, 130(604), 3139–3172,
1184 doi:10.1256/qj.03.145, 2004.
- 1185 Guillod, B.P., Orlowsky, B., Miralles, D., Teuling, A.J., Blanken, P.D., Buchmann, N.,
1186 Ciais, P., Ek, M., Findell, K.L., Gentine, P. and Lintner, B.R., Land-surface controls
1187 on afternoon precipitation diagnosed from observational data: uncertainties and
1188 confounding factors, *Atmos. Chem. Phys*, 14(16), 8343–8367, doi:10.5194/acp-14-
1189 8343-2014-supplement, 2014.
- 1190 Guillod, B. P., B. Orlowsky, D. G. Miralles, A. J. Teuling, and S. I. Seneviratne,
1191 Reconciling spatial and temporal soil moisture effects on afternoon rainfall, *Nat*
1192 *Comms*, 6, 6443, doi:10.1038/ncomms7443, 2015.
- 1193 H. G. Ouwersloot, M. Sikma, C. M. J. Jacobs, J. V.-G. de Arellano, X. Pedruzo-
1194 Bagazgoitia, M. Sikma, and C. C. van Heerwaarden, Direct and Diffuse Radiation in
1195 the Shallow Cumulus–Vegetation System: Enhanced and Decreased
1196 Evapotranspiration Regimes, *J Hydrometeorol*, 18(6), 1731–1748, doi:10.1175/JHM-
1197 D-16-0279.1, 2017.
- 1198 Hadden, D., and A. Grelle, Changing temperature response of respiration turns boreal
1199 forest from carbon sink into carbon source, *Agr Forest Meteorol*, 223, 30–38,
1200 doi:10.1016/j.agrformet.2016.03.020, 2016.



- 1201 Hamada, J.-I., M. D. Yamanaka, S. Mori, Y. I. Tauhid, and T. Sribimawati, Differences
1202 of Rainfall Characteristics between Coastal and Interior Areas of Central Western
1203 Sumatera, Indonesia, *Journal of the Meteorological Society of Japan. Ser. II*, 86(5),
1204 593–611, doi:10.2151/jmsj.86.593, 2008.
- 1205 Han, X., H.-J. H. Franssen, C. Montzka, and H. Vereecken, Soil moisture and soil
1206 properties estimation in the Community Land Model with synthetic brightness
1207 temperature observations, *Water resources Research*, n/a–n/a,
1208 doi:10.1002/2013WR014586, 2014.
- 1209 Haverd, V., M. Cuntz, L. P. Nieradzic, and I. N. Harman, Improved representations of
1210 coupled soil-canopy processes in the CABLE land surface model, *Geosci. Model
1211 Dev. Discuss.*, 1–24, doi:10.5194/gmd-2016-37, 2016.
- 1212 Grant, L. D., & van den Heever, S. C., Cold pool dissipation. *Journal of Geophysical
1213 Research: Atmospheres*, 121(3), 1138–1155, 2016.
- 1214 Heroult, A., Y. LIN, and A. Bourne, Optimal stomatal conductance in relation to
1215 photosynthesis in climatically contrasting Eucalyptus species under drought, *Plant
1216 Cell and Env*, doi:10.1111/j.1365-3040.2012.02570.x, 2013.
- 1217 Hidayat, R., and S. Kizu, Influence of the Madden-Julian Oscillation on Indonesian
1218 rainfall variability in austral summer, *Int J Climatol*, 23(12), n/a–n/a,
1219 doi:10.1002/joc.2005, 2009.
- 1220 Hilker, T., A. I. Lyapustin, C. J. Tucker, F. G. Hall, R. B. Myneni, Y. Wang, J. Bi, Y.
1221 Mendes de Moura, and P. J. Sellers, Vegetation dynamics and rainfall sensitivity of
1222 the Amazon, *Proceedings of the National Academy of Sciences*, 111(45), 16041–
1223 16046, doi:10.1073/pnas.1404870111, 2014.
- 1224 Hohenegger, C., and C. S. Bretherton, Simulating deep convection with a shallow
1225 convection scheme, *Atmos. Chem. Phys*, 11(20), 10389–10406, doi:10.5194/acp-11-
1226 10389-2011, 2011.



- 1227 Horn, G. L., H. G. Ouwersloot, J. V.-G. de Arellano, and M. Sikma, Cloud Shading
1228 Effects on Characteristic Boundary-Layer Length Scales, *Bound-Lay Meteorol*,
1229 *157*(2), 237–263, doi:10.1007/s10546-015-0054-4, 2015.
- 1230 Huang, R., and F. Sun, Impacts of the Tropical Western Pacific on the East Asian
1231 Summer Monsoon, *Journal of the Meteorological Society of Japan. Ser. II*, *70*(1B),
1232 243–256, doi:10.2151/jmsj1965.70.1B_243, 1992.
- 1233 Huete, A. R., K. Didan, Y. E. Shimabukuro, P. Ratana, S. R. Saleska, L. R. Hutyrá, W.
1234 Yang, R. R. Nemani, and R. Myneni (2006), Amazon rainforests green-up with
1235 sunlight in dry season, *Geophys Res Lett*, *33*(6), L06405,
1236 doi:10.1029/2005GL025583, 2006.
- 1237 Huffman, G. J., R. F. Adler, M. M. Morrissey, D. T. Bolvin, S. Curtis, R. Joyce, B.
1238 McGavock, and J. Susskind, Global precipitation at one-degree daily resolution from
1239 multisatellite observations, *J Hydrometeorol*, *2*(1), 36–50, doi:10.1175/1525-
1240 7541(2001)002<0036:GPAODD>2.0.CO;2, 2001.
- 1241 Huijnen, V., M. J. Wooster, J. W. Kaiser, D. L. A. Gaveau, J. Flemming, M. Parrington,
1242 A. Inness, D. Murdiyarso, B. Main, and M. van Weele, Fire carbon emissions over
1243 maritime southeast Asia in 2015 largest since 1997, *Sci. Rep.*, 1–8,
1244 doi:10.1038/srep26886, 2016.
- 1245 Jardine, K., Chambers, J., Alves, E.G., Teixeira, A., Garcia, S., Holm, J., Higuchi, N.,
1246 Manzi, A., Abrell, L., Fuentes, J.D. and Nielsen, L.K., Dynamic Balancing of
1247 Isoprene Carbon Sources Reflects Photosynthetic and Photorespiratory Responses to
1248 Temperature Stress, *Plant Physiol*, *166*(4), 2051–2064, doi:10.1104/pp.114.247494,
1249 2014.
- 1250 Jimenez, C., Prigent, C., Mueller, B., Seneviratne, S.I., McCabe, M.F., Wood, E.F.,
1251 Rossow, W.B., Balsamo, G., Betts, A.K., Dirmeyer, P.A. and Fisher, J.B., Global
1252 intercomparison of 12 land surface heat flux estimates, *J Geophys Res*, *116*(D2),
1253 1147–27, doi:10.1029/2010JD014545, 2011.



- 1254 Joiner, J., A. P. Vasilkov, Y. Yoshida, L. A. Corp, and E. M. Middleton, First
1255 observations of global and seasonal terrestrial chlorophyll fluorescence from space,
1256 *Biogeosciences*, 8(3), 637–651, doi:10.5194/bg-8-637-2011, 2011.
- 1257 Joiner, J., L. Guanter, R. Lindstrot, M. Voigt, A. P. Vasilkov, E. M. Middleton, K. F.
1258 Huemmrich, Y. Yoshida, and C. Frankenberg, Global monitoring of terrestrial
1259 chlorophyll fluorescence from moderate-spectral-resolution near-infrared satellite
1260 measurements: methodology, simulations, and application to GOME-2, *Atmos Meas*
1261 *Tech*, 6(10), 2803–2823, doi:10.5194/amt-6-2803-2013, 2013.
- 1262 Juárez, R. I. N., M. G. Hodnett, R. Fu, M. L. Goulden, and C. von Randow, Control of
1263 Dry Season Evapotranspiration over the Amazonian Forest as Inferred from
1264 Observations at a Southern Amazon Forest Site, *J Climate*, 20(12), 2827–2839,
1265 doi:10.1175/JCLI4184.1, 2007.
- 1266 Jung, M., Reichstein, M., Schwalm, C.R., Huntingford, C., Sitch, S., Ahlström, A.,
1267 Arneth, A., Camps-Valls, G., Ciais, P., Friedlingstein, P. and Gans, F., Compensatory
1268 water effects link yearly global land CO₂ sink changes to temperature., *541*(7638),
1269 516–520, doi:10.1038/nature20780, 2017.
- 1270 Kato, S., N. G. Loeb, F. G. Rose, D. R. Doelling, D. A. Rutan, T. E. Caldwell, L. Yu, and
1271 R. A. Weller, Surface Irradiances Consistent with CERES-Derived Top-of-
1272 Atmosphere Shortwave and Longwave Irradiances, *J Climate*, 26(9), 2719–2740,
1273 doi:10.1175/JCLI-D-12-00436.1, 2013.
- 1274 Keller, M., Alencar, A., Asner, G.P., Braswell, B., Bustamante, M., Davidson, E.,
1275 Feldpausch, T., Fernandes, E., Goulden, M., Kabat, P. and Kruijt, B., Ecological
1276 Research in the Large-Scale Biosphere– Atmosphere Experiment in Amazonia: Early
1277 Results, *Ecol Appl*, 14(sp4), 3–16, 2004.
- 1278 Kennedy, D., P. Gentine, R. A. Fisher, and D. M. Lawrence, Implementation of plant
1279 hydraulics in the Community Land Model, *JAMES*, 2017.
- 1280 Khairoutdinov, M., and D. Randall, High-resolution simulation of shallow-to-deep
1281 convection transition over land, *J Atmos Sci*, 63(12), 3421–3436, 2006.



- 1282 Khanna, J., D. Medvigy, S. Fueglistaler, and R. Walko, Regional dry-season climate
1283 changes due to three decades of Amazonian deforestation, *Nature Climate Change*,
1284 7(3), 200–204, doi:10.1038/nclimate3226, 2017.
- 1285 Knox, R. G., M. Longo, A. L. S. Swann, K. Zhang, N. M. Levine, P. R. Moorcroft, and
1286 R. L. Bras, Hydrometeorological effects of historical land-conversion in an
1287 ecosystem-atmosphere model of Northern South America, *Hydrol Earth Syst Sc*,
1288 19(1), 241–273, doi:10.5194/hess-19-241-2015, 2015.
- 1289 Konings, A. G., and P. Gentine, Global variations in ecosystem-scale isohydricity, *Global*
1290 *Change Biol*, doi:10.1111/gcb.13389, 2016.
- 1291 Koren, I., Y. J. Kaufman, L. A. Remer, and J. V. Martins, Measurement of the effect of
1292 Amazon smoke on inhibition of cloud formation, *Science*, 303(5662), 1342–1345,
1293 doi:10.1126/science.1089424, 2004.
- 1294 Koster, R.D., Dirmeyer, P.A., Guo, Z., Bonan, G., Chan, E., Cox, P., Gordon, C.T.,
1295 Kanae, S., Kowalczyk, E., Lawrence, D. and Liu, P., Regions of strong coupling
1296 between soil moisture and precipitation, *Science*, 305(5687), 1138–1140, 2004.
- 1297 Koster, R.D., Dirmeyer, P.A., Guo, Z., Bonan, G., Chan, E., Cox, P., Gordon, C.T.,
1298 Kanae, S., Kowalczyk, E., Lawrence, D. and Liu, P., The Second Phase of the Global
1299 Land–Atmosphere Coupling Experiment: Soil Moisture Contributions to Subseasonal
1300 Forecast Skill, *J Hydrometeorol*, 12(5), 805–822, doi:10.1175/2011JHM1365.1,
1301 2011.
- 1302 Köppen, W., *The thermal zones of the Earth according to the duration of hot, moderate*
1303 *and cold periods and of the impact of heat on the organic world.(translated and ...*,
1304 *Meteorologische Zeitschrift*, 1884.
- 1305 Krakauer, N. Y., M. J. Puma, B. I. Cook, P. Gentine, and L. Nazarenko, Ocean-
1306 atmosphere interactions modulate irrigation's climate impacts,, 1–16,
1307 doi:10.5194/esd-2016-23, 2016.



- 1308 Kuang, Z., Linear response functions of a cumulus ensemble to temperature and moisture
1309 perturbations and implications for the dynamics of convectively coupled waves, *J*
1310 *Atmos Sci*, 2010.
- 1311 Kuang, Z., A Moisture-Stratiform Instability for Convectively Coupled Waves, *Journal*
1312 *of Atmospheric Sciences*, 65(3), 834–854, doi:10.1175/2007JAS2444.1, 2008.
- 1313 Laan-Luijkx, I.T., Velde, I.R., Krol, M.C., Gatti, L.V., Domingues, L.G., Correia, C.S.C.,
1314 Miller, J.B., Gloor, M., Leeuwen, T.T., Kaiser, J.W. and Wiedinmyer, C., Response
1315 of the Amazon carbon balance to the 2010 drought derived with CarbonTracker
1316 South America, *Global Biogeochem Cy*, 29(7), 1092–1108,
1317 doi:10.1002/2014GB005082, 2015.
- 1318 Laurent, H., L. Machado, and C. A. Morales, Characteristics of the Amazonian mesoscale
1319 convective systems observed from satellite and radar during the WETAMC/LBA
1320 experiment, *J of Climate*, 2002.
- 1321 Lawrence, D. M., K. W. Oleson, and M. G. Flanner, Parameterization improvements and
1322 functional and structural advances in Version 4 of the Community Land Model,
1323 *JAMES*, 2011
- 1324 Lawrence, D., and K. Vandecar, Effects of tropical deforestation on climate and
1325 agriculture, *Nature Climate Change*, 5(1), 27–36, doi:10.1038/nclimate2430, 2015.
- 1326 Lawton, R. O., U. S. Nair, R. A. Pielke Sr, and R. M. Welch, Climatic Impact of Tropical
1327 Lowland Deforestation on Nearby Montane Cloud Forests, *Science*, 294, 584–587,
1328 2001.
- 1329 Lebel, T., Cappelaere, B., Galle, S., Hanan, N., Kergoat, L., Levis, S., Vieux, B.,
1330 Descroix, L., Gosset, M., Mougin, E. and Peugeot, C., AMMA-CATCH studies in
1331 the Sahelian region of West-Africa: An overview, *Journal of Hydrology*, 375(1-2),
1332 3–13, doi:10.1016/j.jhydrol.2009.03.020, 2009.
- 1333 Lee, J. E., R. S. Oliveira, T. E. Dawson, and I. Fung, Root functioning modifies seasonal
1334 climate, *P Natl Acad Sci Usa*, 102(49), 17576–17581, 2005.



- 1335 Lee, J.-E., J. A. Berry, C. van der Tol, X. Yang, L. Guanter, A. Damm, I. Baker, and C.
1336 Frankenberg, Simulations of chlorophyll fluorescence incorporated into the
1337 Community Land Model version 4, *Global Change Biol*, n/a–n/a,
1338 doi:10.1111/gcb.12948, 2015.
- 1339 Lemordant, L., Modification of land-atmosphere interactions by CO₂ effects:
1340 Implications for summer dryness and heat wave amplitude, *Geo Res Letters*, 43(19),
1341 10–240–10–248, doi:10.1002/2016GL069896, 2016.
- 1342 Leuning, R., A critical appraisal of a combined stomatal-photosynthesis model for C3
1343 plants, *Plant Cell and Env*, 1995.
- 1344 Leuning, R., F. M. Kelliher, D. G. G. PURY, and E. D. Schulze, Leaf nitrogen,
1345 photosynthesis, conductance and transpiration: scaling from leaves to canopies, *Plant*
1346 *Cell Environ*, 18(10), 1183–1200, doi:10.1111/j.1365-3040.1995.tb00628.x, 1995.
- 1347 Levy, M. C., A. Cohn, A. V. Lopes, and S. E. Thompson, Addressing rainfall data
1348 selection uncertainty using connections between rainfall and streamflow, *Sci. Rep.*,
1349 7(1), 1–12, doi:10.1038/s41598-017-00128-5, 2017.
- 1350 Li, W., R. Fu, and R. E. Dickinson, Rainfall and its seasonality over the Amazon in the
1351 21st century as assessed by the coupled models for the IPCC AR4, *Journal of*
1352 *Geophysical Research*, 2006.
- 1353 Liebmann, B., and J. A. Marengo, Interannual variability of the rainy season and rainfall
1354 in the Brazilian Amazon basin, *J Climate*, 14(22), 4308–4318, 2001.
- 1355 Lintner, B. R., and J. Chiang, Reorganization of tropical climate during El Nino: A weak
1356 temperature gradient approach, *J Climate*, 18(24), 5312–5329, 2005.
- 1357 Lintner, B. R., and J. D. Neelin, A prototype for convective margin shifts, *Geophys Res*
1358 *Lett*, 34(5), L05812, doi:10.1029/2006GL027305, 2007.
- 1359 Lintner, B. R., and J. D. Neelin, Soil Moisture Impacts on Convective Margins, *J*
1360 *Hydrometeorol*, 10(4), 1026–1039, doi:10.1175/2009JHM1094.1, 2009.



- 1361 Lintner, B. R., P. Gentine, K. L. Findell, and G. D. Salvucci, The Budyko and
1362 complementary relationships in an idealized model of large-scale land–atmosphere
1363 coupling, *Hydrol Earth Syst Sc*, 19(5), 2119–2131, doi:10.5194/hess-19-2119-2015,
1364 2015.
- 1365 Lintner, B. R., P. Gentine, K. L. Findell, F. D'Andrea, A. H. Sobel, and G. D. Salvucci,
1366 An idealized prototype for large-scale land-atmosphere coupling, *J Climate*, 26(7),
1367 2379–2389, doi:10.1175/JCLI-D-11-00561.1, 2013.
- 1368 Liu, L., L. Guan, and X. Liu, Directly estimating diurnal changes in GPP for C3 and C4
1369 crops using far-red sun-induced chlorophyll fluorescence, *Agr Forest Meteorol*, 232,
1370 1–9, doi:10.1016/j.agrformet.2016.06.014, 2017.
- 1371 Lohou, F., F. Said, M. Lothon, P. Durand, and D. Serça, Impact of Boundary-Layer
1372 Processes on Near-Surface Turbulence Within the West African Monsoon, *Bound-
1373 Lay Meteorol*, 136(1), 1–23, doi:10.1007/s10546-010-9493-0, 2010.
- 1374 Lopes, A. P., B. W. Nelson, J. Wu, P. M. L. de Alencastro Graça, J. V. Tavares, N.
1375 Prohaska, G. A. Martins, and S. R. Saleska, Leaf flush drives dry season green-up of
1376 the Central Amazon, *Remote Sensing of Environment*, 182(C), 90–98,
1377 doi:10.1016/j.rse.2016.05.009, 2016.
- 1378 Machado, L.A., Silva Dias, M.A., Morales, C., Fisch, G., Vila, D., Albrecht, R.,
1379 Goodman, S.J., Calheiros, A.J., Biscaro, T., Kummerow, C. and Cohen, J.. The
1380 CHUVA project: How does convection vary across Brazil?. *Bulletin of the American
1381 Meteorological Society*, 95(9), 1365-1380, 2014.
- 1382 Machado, L., and H. Laurent, Diurnal march of the convection observed during TRMM-
1383 WETAMC/LBA, *J Geo Res: Atmo*, 2002.
- 1384 Mahecha, M. D. et al., Global convergence in the temperature sensitivity of respiration at
1385 ecosystem level, *Science*, 329(5993), 838–840, doi:10.1126/science.1189587, 2010.



- 1386 Marengo, J. A., J. Tomasella, L. M. Alves, W. R. Soares, and D. A. Rodriguez, The
1387 drought of 2010 in the context of historical droughts in the Amazon region, *Geophys*
1388 *Res Lett*, 38(12), n/a–n/a, doi:10.1029/2011GL047436, 2011.
- 1389 Martin, S.T., Artaxo, P., Machado, L.A.T., Manzi, A.O., Souza, R.A.F., Schumacher, C.,
1390 Wang, J., Andreae, M.O., Barbosa, H.M.J., Fan, J. and Fisch, G., Introduction:
1391 Observations and Modeling of the Green Ocean Amazon (GoAmazon2014/5),
1392 *Atmos. Chem. Phys*, 16(8), 4785–4797, doi:10.5194/acp-16-4785-2016, 2016.
- 1393 Martin, S. T. et al., The Green Ocean Amazon Experiment (GoAmazon2014/5) Observes
1394 Pollution Affecting Gases, Aerosols, Clouds, and Rainfall over the Rain Forest, *Bull.*
1395 *Amer. Meteor. Soc.*, 98(5), 981–997, doi:10.1175/BAMS-D-15-00221.1, 2017.
- 1396 Martinez-Vilalta, J., and N. Garcia-Forner, Water potential regulation, stomatal
1397 behaviour and hydraulic transport under drought: deconstructing the iso/anisohydric
1398 concept, *Plant Cell Environ*, 40(6), 962–976, doi:10.1111/pce.12846, 2016.
- 1399 Martinez-Vilalta, J., R. Poyatos, D. Aguadé, J. Retana, and M. Mencuccini, A new look
1400 at water transport regulation in plants, *New Phytologist*, doi:10.1111/nph.12912,
1401 2014.
- 1402 Medlyn, B. E., R. A. Duursma, D. Eamus, D. S. Ellsworth, I. C. Prentice, C. V. M.
1403 Barton, K. Y. Crous, P. De Angelis, M. Freeman, and L. Wingate, Reconciling the
1404 optimal and empirical approaches to modelling stomatal conductance, *Global*
1405 *Change Biol*, 17(6), 2134–2144, doi:10.1111/j.1365-2486.2010.02375.x, 2011.
- 1406 Medlyn, B. E., R. A. Duursma, D. Eamus, D. S. Ellsworth, I. Colin Prentice, C. V. M.
1407 Barton, K. Y. Crous, P. Angelis, M. Freeman, and L. Wingate, Reconciling the
1408 optimal and empirical approaches to modelling stomatal conductance, *Global*
1409 *Change Biol*, 18(11), 3476–3476, doi:10.1111/j.1365-2486.2012.02790.x, 2012.
- 1410 Medvigy, D., R. L. Walko, and R. Avissar, Effects of Deforestation on Spatiotemporal
1411 Distributions of Precipitation in South America, *J Climate*, 24, 2147–2163, 2011.



- 1412 Miralles, D. G., J. H. Gash, T. R. H. Holmes, R. A. M. de Jeu, and A. J. Dolman, Global
1413 canopy interception from satellite observations, *J Geophys Res*, 115(D16), 237,
1414 doi:10.1029/2009JD013530, 2010.
- 1415 Morton, D. C., and B. D. Cook, Amazon forest structure generates diurnal and seasonal
1416 variability in light utilization, *Biogeosciences*, 13(7), 2195–2206, doi:10.5194/bg-13-
1417 2195-2016, 2016.
- 1418 Morton, D. C., J. Nagol, C. C. Carabajal, J. Rosette, M. Palace, B. D. Cook, E. F.
1419 Vermote, D. J. Harding, and P. R. J. North, Amazon forests maintain consistent
1420 canopy structure and greenness during the dry season, *Nature*, 506(7487), 221–224,
1421 doi:10.1038/nature13006, 2014.
- 1422 Mueller, B., Seneviratne, S.I., Jimenez, C., Corti, T., Hirschi, M., Balsamo, G., Ciais, P.,
1423 Dirmeyer, P., Fisher, J.B., Guo, Z. and Jung, M., Evaluation of global observations-
1424 based evapotranspiration datasets and IPCC AR4 simulations, *Geophys Res Lett*, 38,
1425 –, doi:10.1029/2010GL046230, 2011.
- 1426 Munger, J. W., J. B. McManus, D. D. Nelson, M. S. Zahniser, E. A. Davidson, S. C.
1427 Wofsy, R. Wehr, and S. R. Saleska, Seasonality of temperate forest photosynthesis
1428 and daytime respiration, *Nature*, 534(7609), 680–683, doi:10.1038/nature17966,
1429 2016.
- 1430 Nakicenovic, N., IPCC Special Report on Emissions Scenarios, 2000
- 1431 Naudts, K., Ryder, J., McGrath, M.J., Otto, J., Chen, Y., Valade, A., Bellasen, V.,
1432 Berhongaray, G., Bönisch, G., Campioli, M. and Ghattas, J., A vertically discretised
1433 canopy description for ORCHIDEE (SVN r2290) and the modifications to the
1434 energy, water and carbon fluxes, *Geosci. Model Dev. Discuss.*, 7(6), 8565–8647,
1435 doi:10.5194/gmdd-7-8565-2014, 2014.
- 1436 Ngo-Duc, T., K. Laval, G. Ramillien, J. Polcher, and A. Cazenave, Validation of the land
1437 water storage simulated by Organising Carbon and Hydrology in Dynamic
1438 Ecosystems (ORCHIDEE) with Gravity Recovery and Climate Experiment



- 1439 (GRACE) data, *Water resources Research*, 43(4), –, doi:10.1029/2006WR004941,
1440 2007.
- 1441 Nicholson, S., Land surface processes and Sahel climate, *Rev Geophys*, 38(1), 117–139,
1442 2000.
- 1443 Nitta, T., Convective Activities in the Tropical Western Pacific and Their Impact on the
1444 Northern Hemisphere Summer Circulation, *Journal of the Meteorological Society of*
1445 *Japan. Ser. II*, 65(3), 373–390, doi:10.2151/jmsj1965.65.3_373, 1987.
- 1446 Naudts, K., Ryder, J., McGrath, M.J., Otto, J., Chen, Y., Valade, A., Bellasen, V.,
1447 Berhongaray, G., Bönisch, G., Campioli, M. and Ghattas, J., The community Noah
1448 land surface model with multiparameterization options (Noah-MP): 1. Model
1449 description and evaluation with local-scale measurements, *J Geophys Res-Atmos*,
1450 116, –, doi:10.1029/2010JD015139, 2011.
- 1451 Noilhan, J., and S. Planton, A simple parameterization of land surface processes for
1452 meteorological models, *Mon Wea Rev*, 1989.
- 1453 Oleson, K.W., Niu, G.Y., Yang, Z.L., Lawrence, D.M., Thornton, P.E., Lawrence, P.J.,
1454 Stöckli, R., Dickinson, R.E., Bonan, G.B., Levis, S. and Dai, A., Improvements to the
1455 Community Land Model and their impact on the hydrological cycle, *J Geophys Res-*
1456 *Biogeo*, 113, –, doi:10.1029/2007JG000563, 2008.
- 1457 Oliveira, R. S., T. E. Dawson, S. S. O. Burgess, and D. C. Nepstad, Hydraulic
1458 redistribution in three Amazonian trees, *Oecologia*, 145(3), 354–363,
1459 doi:10.1007/s00442-005-0108-2, 2005.
- 1460 Ouwersloot, H. G., J. V.-G. de Arellano, B. J. H. van Stratum, M. C. Krol, and J.
1461 Lelieveld, Quantifying the transport of sub-cloud layer reactants by shallow cumulus
1462 clouds over the Amazon, *J Geophys Res-Atmos*, n/a–n/a,
1463 doi:10.1002/2013JD020431, 2013.
- 1464 Park, S., and C. S. Bretherton, The University of Washington Shallow Convection and
1465 Moist Turbulence Schemes and Their Impact on Climate Simulations with the



- 1466 Community Atmosphere Model, *J Climate*, 22(12), 3449–3469,
1467 doi:10.1175/2008JCLI2557.1, 2009.
- 1468 Park, S.-B., S. Boeing, and P. Gentine, Role of shear on shallow convection (in press), *J*
1469 *Atmos Science*, 2018.
- 1470 Peterhansel, C., and V. G. Maurino, Photorespiration Redesign, *Plant Physiol*, 155(1),
1471 49–55, doi:10.1104/pp.110.165019, 2011.
- 1472 Phillips, N. G., R. Oren, J. Licata, and S. Linder, Time series diagnosis of tree hydraulic
1473 characteristics, *Tree Physiol*, 879–890, 2004.
- 1474 Phillips, N. G., T. N. Buckley, and D. T. Tissue, Capacity of Old Trees to Respond to
1475 Environmental Change, *Journal of Integrative Plant Biology*, 50(11), 1355–1364,
1476 doi:10.1111/j.1744-7909.2008.00746.x, 2008.
- 1477 Phillips, N., A. Nagchaudhuri, R. Oren, and G. Katul, Time constant for water transport
1478 in loblolly pine trees estimated from time series of evaporative demand and stem
1479 sapflow, *Trees*, 11(7), 412–419, 1997.
- 1480 Pielke Sr, R.A., Pitman, A., Niyogi, D., Mahmood, R., McAlpine, C., Hossain, F.,
1481 Goldewijk, K.K., Nair, U., Betts, R., Fall, S. and Reichstein, M., Land use/land
1482 cover changes and climate: modeling analysis and observational evidence, *Wires*
1483 *Clim Change*, 2(6), 828–850, doi:10.1002/wcc.144, 2011.
- 1484 Pielke, R. A., Sr, R. Mahmood, and C. McAlpine, Land’s complex role in climate
1485 change, *Physics Today*, 69(11), 40–46, doi:10.1063/PT.3.3364, 2016.
- 1486 Pielke, R., and R. Avissar, Influence of landscape structure on local and regional climate,
1487 *Landscape Ecology*, 4(2/3), 133–155, 1990.
- 1488 Pielke, R., G. DALU, J. SNOOK, T. LEE, and T. KITTEL, Nonlinear Influence of
1489 Mesoscale Land-Use on Weather and Climate, *J Climate*, 4(11), 1053–1069, 1991.
- 1490 Pons, T. L., and R. Welschen, Midday depression of net photosynthesis in the tropical
1491 rainforest tree *Eperua grandiflora*: contributions of stomatal and internal



- 1492 conductances, respiration and Rubisco functioning, *Tree Physiol*, 23(14), 937–947,
1493 2003.
- 1494 Poulter, B., Frank, D., Ciais, P., Myneni, R.B., Andela, N., Bi, J., Broquet, G., Canadell,
1495 J.G., Chevallier, F., Liu, Y.Y. and Running, S.W., Contribution of semi-arid
1496 ecosystems to interannual variability of the global carbon cycle, *Nature*, 509(7502),
1497 600–603, doi:10.1038/nature13376, 2014.
- 1498 Powell, T.L., Galbraith, D.R., Christoffersen, B.O., Harper, A., Imbuzeiro, H.M.,
1499 Rowland, L., Almeida, S., Brando, P.M., da Costa, A.C.L., Costa, M.H. and Levine,
1500 N.M., Confronting model predictions of carbon fluxes with measurements of
1501 Amazon forests subjected to experimental drought, *New Phytologist*, 200(2), 350–
1502 365, doi:10.1111/nph.12390, 2013.
- 1503 Pradipta, P., A. Giannini, P. Gentine, and U. Lall, Resolving Contrasting Regional
1504 Rainfall Responses to El Niño over Tropical Africa, *J Climate*, 29(4), 1461–1476,
1505 doi:10.1175/JCLI-D-15-0071.1, 2016.
- 1506 Prieto, I., and R. J. Ryel, Internal hydraulic redistribution prevents the loss of root
1507 conductivity during drought, *Tree Physiol*, 34(1), 39–48,
1508 doi:10.1093/treephys/tpt115, 2014.
- 1509 Ray, D. K., U. S. Nair, R. O. Lawton, R. M. Welch, and R. A. Pielke Sr. Impact of land
1510 use on Costa Rican tropical montane cloud forests: Sensitivity of orographic cloud
1511 formation to deforestation in the plains, *J Geophys Res*, 111(D2), D02108,
1512 doi:10.1029/2005JD006096, 2006.
- 1513 Raymond, D. J., and X. Zeng, Modelling tropical atmospheric convection in the context
1514 of the weak temperature gradient approximation, *Q J Roy Meteor Soc*, 131(608),
1515 1301–1320, doi:10.1256/qj.03.97, 2005.
- 1516 Redelsperger, J.-L., C. D. Thorncroft, A. Diedhiou, T. Lebel, D. J. Parker, and J. Polcher
1517 African monsoon multidisciplinary analysis - An international research project and
1518 field campaign, *Bull. Amer. Meteor. Soc.*, 87(12), 1739–+, doi:10.1175/BAMS-87-
1519 12-1739, 2006.



- 1520 Restrepo-Coupe, N., da Rocha, H.R., Hutyra, L.R., da Araujo, A.C., Borma, L.S.,
1521 Christoffersen, B., Cabral, O.M., de Camargo, P.B., Cardoso, F.L., da Costa, A.C.L.
1522 and Fitzjarrald, D.R., What drives the seasonality of photosynthesis across the
1523 Amazon basin? A cross-site analysis of eddy flux tower measurements from the
1524 Brasil flux network, *Agr Forest Meteorol*, 182-183, 128–144,
1525 doi:10.1016/j.agrformet.2013.04.031, 2013.
- 1526 Rieck, M., C. Hohenegger, and C. C. van Heerwaarden, The influence of land surface
1527 heterogeneities on cloud size development, *Mon Wea Rev*, 140611124045000,
1528 doi:10.1175/MWR-D-13-00354.1, 2014.
- 1529 Rieck, M., C. Hohenegger, and P. Gentine, The effect of moist convection on thermally
1530 induced mesoscale circulations, *Q J Roy Meteor Soc*, 141(691), 2418–2428,
1531 doi:10.1002/qj.2532, 2015.
- 1532 Rio, C., F. Hourdin, J. Y. Grandpeix, and J. P. Lafore, Shifting the diurnal cycle of
1533 parameterized deep convection over land, *Geophys Res Lett*, 36, –,
1534 doi:10.1029/2008GL036779, 2009.
- 1535 Rochetin, N., F. Couvreux, J.-Y. Grandpeix, and C. Rio, Deep Convection Triggering by
1536 Boundary Layer Thermals. Part I: LES Analysis and Stochastic Triggering
1537 Formulation, *J Atmos Sci*, 71(2), 496–514, doi:10.1175/JAS-D-12-0336.1, 2014.
- 1538 Rochetin, N., J.-Y. Grandpeix, C. Rio, and F. Couvreux, Deep Convection Triggering by
1539 Boundary Layer Thermals. Part II: Stochastic Triggering Parameterization for the
1540 LMDZ GCM, *J Atmos Sci*, 71(2), 515–538, doi:10.1175/JAS-D-12-0337.1, 2014.
- 1541 Romps, D. M., Numerical tests of the weak pressure gradient approximation, *J Atmos Sci*,
1542 69(9), 2846–2856, doi:10.1175/JAS-D-11-0337.1, 2012.
- 1543 Romps, D. M., Weak Pressure Gradient Approximation and Its Analytical Solutions, *J*
1544 *Atmos Sci*, 69(9), 2835–2845, doi:10.1175/JAS-D-11-0336.1, 2012.
- 1545 Roy, S., C. Weaver, D. Nolan, and R. Avissar, A preferred scale for landscape forced
1546 mesoscale circulations? *J Geophys Res-Atmos*, 108(D22), 8854,
1547 doi:10.1029/2002JD003097, 2003.



- 1548 Saatchi, S., S. Asefi-Najafabady, Y. Malhi, L. E. O. C. Aragao, L. O. Anderson, R. B.
1549 Myneni, and R. Nemani, Persistent effects of a severe drought on Amazonian forest
1550 canopy, *PNAS*, *110*(2), 565–570, doi:10.1073/pnas.1204651110, 2013.
- 1551 Saleska, S. R., J. Wu, K. Guan, A. C. Araujo, and A. Huete, Dry-season greening of
1552 Amazon forests, *Nature*, doi:10.1038/nature16457, 2016.
- 1553 Schaeffli, B., R. J. van der Ent, R. Woods, and H. H. G. Savenije, An analytical model for
1554 soil-atmosphere feedback, *Hydrol Earth Syst Sc*, *16*(7), 1863–1878,
1555 doi:10.5194/hess-16-1863-2012, 2012.
- 1556 Schiro, K. A., J. D. Neelin, D. K. Adams, and B. R. Lintner, Deep Convection and
1557 Column Water Vapor over Tropical Land versus Tropical Ocean: A Comparison
1558 between the Amazon and the Tropical Western Pacific, *Journal of Atmospheric*
1559 *Sciences*, *73*(10), 4043–4063, doi:10.1175/JAS-D-16-0119.1, 2016.
- 1560 Scholz, F., N. Phillips, and S. Bucci, Hydraulic capacitance: biophysics and functional
1561 significance of internal water sources in relation to tree size, *Size- and Age-Related*
1562 *Changes in Tree Structure*, 341–361, 2011.
- 1563 Scott, R., D. Entekhabi, R. D. Koster, and M. Suarez, Timescales of land surface
1564 evapotranspiration response, *J Climate*, *10*(4), 559–566, 1997.
- 1565 Sellers, P. J., C. J. Tucker, G. J. Collatz, S. O. Los, C. O. Justice, D. A. Dazlich, and D.
1566 A. Randall, A Revised Land Surface Parameterization (SiB2) for Atmospheric
1567 GCMS. Part II: The Generation of Global Fields of Terrestrial Biophysical
1568 Parameters from Satellite Data, *J Climate*, *9*(4), 706–737, doi:10.1175/1520-
1569 0442(1996)009<0706:ARLSPF>2.0.CO;2, 1996.
- 1570 Sellers, P., D. A. Randall, G. Collatz, J. Berry, C. Field, D. Dazlich, C. Zhang, G.
1571 Collelo, and L. Bounoua, A Revised Land Surface Parameterization (SiB2) for
1572 Atmospheric GCMS. Part I: Model Formulation, *J Climate*, *9*(4), 676–705, 1996.
- 1573 Seneviratne, S., Impact of soil moisture-climate feedbacks on CMIP5 projections: First
1574 results from the GLACE-CMIP5 experiment, *Geophys Res Lett*, *40*(19), 5212–5217,
1575 doi:10.1002/grl.50956, 2013.



- 1576 Sentić, S., and S. L. Sessions, Idealized modeling of convective organization with
1577 Changing Sea surface temperatures using multiple equilibria in weak temperature
1578 gradient simulations, *J. Adv. Model. Earth Syst.*, 1–65, doi:10.1002/2016MS000873,
1579 2017.
- 1580 Sobel, A. H., and C. S. Bretherton, Large-scale waves interacting with deep convection in
1581 idealized mesoscale model simulations, *Tellus Series A-Dynamic Meteorology And*
1582 *Oceanography*, 55(1), 45–60, doi:10.1034/j.1600-0870.2003.201421.x, 2003.
- 1583 Sobel, A. H., G. Bellon, and J. Bacmeister, Multiple equilibria in a single-column model
1584 of the tropical atmosphere, *Geophys Res Lett*, 34(22), L22804,
1585 doi:10.1029/2007GL031320, 2007.
- 1586 Sobel, A. H., J. Nilsson, and L. Polvani, The weak temperature gradient approximation
1587 and balanced tropical moisture waves, *J Atmos Sci*, 58(23), 3650–3665, 2001.
- 1588 Spracklen, D. V., S. R. Arnold, and C. M. Taylor, Observations of increased tropical
1589 rainfall preceded by air passage over forests, *Nature*, 489(7415), 282–285,
1590 doi:10.1038/nature11390, 2012.
- 1591 Stevens, B., and S. Bony, What Are Climate Models Missing? *Science*, 340(6136), 1053–
1592 1054, doi:10.1126/science.1237554, 2013.
- 1593 Stoeckli, R., D. M. Lawrence, G. Y. Niu, K. W. Oleson, P. E. Thornton, Z. L. Yang, G.
1594 B. Bonan, A. S. Denning, and S. W. Running, Use of FLUXNET in the Community
1595 Land Model development, *J Geophys Res*, 113(G1), G01025,
1596 doi:10.1029/2007JG000562, 2008.
- 1597 Sutanto, S. J., J. Wenninger, A. M. J. Coenders-Gerrits, and S. Uhlenbrook, Partitioning
1598 of evaporation into transpiration, soil evaporation and interception: a comparison
1599 between isotope measurements and a HYDRUS-1D model, *Hydrol Earth Syst Sc*,
1600 16(8), 2605–2616, doi:10.5194/hess-16-2605-2012, 2012.
- 1601 Swann, A. L. S., M. Longo, R. G. Knox, E. Lee, and P. R. Moorcroft, Future
1602 deforestation in the Amazon and consequences for South American climate, *Agr*
1603 *Forest Meteorol*, 214-215, 12–24, doi:10.1016/j.agrformet.2015.07.006, 2015.



- 1604 Tang, S., Xie, S., Zhang, Y., Zhang, M., Schumacher, C., Upton, H., Jensen, M.P.,
1605 Johnson, K.L., Wang, M., Ahlgrimm, M. and Feng, Z., Large-scale vertical velocity,
1606 diabatic heating and drying profiles associated with seasonal and diurnal variations of
1607 convective systems observed in the GoAmazon2014/5 experiment, *Atmos. Chem.*
1608 *Phys*, *16*(22), 14249–14264, doi:10.5194/acp-16-14249-2016, 2016.
- 1609 Taylor, C. M., C. E. Birch, D. J. Parker, N. Dixon, F. Guichard, G. Nikulin, and G. M. S.
1610 Lister, New perspectives on land-atmosphere feedbacks from the African Monsoon
1611 Multidisciplinary Analysis, *Atmos Sci Lett*, *12*(1), 38–44, doi:10.1002/asl.336, 2011.
- 1612 Taylor, C. M., C. E. Birch, D. J. Parker, N. Dixon, F. Guichard, G. Nikulin, and G. M. S.
1613 Lister, Modelling soil moisture - precipitation feedbacks in the Sahel: importance of
1614 spatial scale versus convective parameterization, *Geophys Res Lett*, *40*(23), 6213–
1615 6218, doi:10.1002/2013GL058511, 2013.
- 1616 Taylor, C. M., D. J. Parker, and P. P. Harris, An observational case study of mesoscale
1617 atmospheric circulations induced by soil moisture, *Geophys Res Lett*, *34*(15),
1618 L15801, doi:10.1029/2007GL030572, 2007.
- 1619 Taylor, C. M., P. P. Harris, and D. J. Parker, Impact of soil moisture on the development
1620 of a Sahelian mesoscale convective system: a case-study from the AMMA Special
1621 Observing Period, *Q J Roy Meteor Soc*, *136*(S1), 456–470, doi:10.1002/qj.465, 2009.
- 1622 Thiery, W., E. L. Davin, D. M. Lawrence, A. L. Hirsch, M. Hauser, and S. I. Seneviratne,
1623 Present-day irrigation mitigates heat extremes, *J Geophys Res-Atmos*, *122*(3), 1403–
1624 1422, doi:10.1002/2016JD025740, 2017.
- 1625 Thornley, J. H. M., Plant growth and respiration re-visited: maintenance respiration
1626 defined - it is an emergent property of, not a separate process within, the system - and
1627 why the respiration : photosynthesis ratio is conservative, *Annals of Botany*, *108*(7),
1628 1365–1380, doi:10.1093/aob/mcr238, 2011.
- 1629 Thum, T., Zaehle, S., Köhler, P., Aalto, T., Aurela, M., Guanter, L., Kolari, P., Laurila,
1630 T., Lohila, A., Magnani, F. and Tol, C.V.D., Modelling sun-induced fluorescence and



- 1631 photosynthesis with a land surface model at local and regional scales in northern
1632 Europe, *Biogeosciences*, 14(7), 1969–1987, doi:10.5194/bg-14-1969-2017, 2017.
- 1633 Torri, G., Z. Kuang, and Y. Tian, Mechanisms for convection triggering by cold pools,
1634 *Geophys Res Lett*, 42(6), 1943–1950, doi:10.1002/2015GL063227, 2015.
- 1635 van der Ent, R. J., and O. A. Tuinenburg, The residence time of water in the atmosphere
1636 revisited, *Hydrol Earth Syst Sc*, 21(2), 779–790, doi:10.5194/hess-21-779-2017,
1637 2017.
- 1638 van der Ent, R. J., H. H. G. Savenije, B. Schaefli, and S. C. Steele-Dunne, Origin and fate
1639 of atmospheric moisture over continents, *Water resources Research*, 46(9), n/a–n/a,
1640 doi:10.1029/2010WR009127, 2010.
- 1641 van Dijk, A.I., Gash, J.H., van Gorsel, E., Blanken, P.D., Cescatti, A., Emmel, C., Gielen,
1642 B., Harman, I.N., Kiely, G., Merbold, L. and Montagnani, L., Rainfall interception
1643 and the coupled surface water and energy balance, *Agr Forest Meteorol*, 214-215,
1644 402–415, doi:10.1016/j.agrformet.2015.09.006, 2015.
- 1645 Vila-Guerau de Arellano, J., E. G. Patton, T. Karl, K. van den Dries, M. C. Barth, and J.
1646 J. Orlando, The role of boundary layer dynamics on the diurnal evolution of isoprene
1647 and the hydroxyl radical over tropical forests, *J Geophys Res-Atmos*, 116(D7), 8032,
1648 doi:10.1029/2010JD014857, 2011.
- 1649 Vogel, M. M., R. Orth, F. Cheruy, S. Hagemann, R. Lorenz, B. J. J. M. van den Hurk,
1650 and S. I. Seneviratne, Regional amplification of projected changes in extreme
1651 temperatures strongly controlled by soil moisture-temperature feedbacks, *Geophys*
1652 *Res Lett*, 44(3), 1511–1519, doi:10.1002/2016GL071235, 2017.
- 1653 Wang, J., F. J. F. Chagnon, E. R. Williams, A. K. Betts, N. O. Renno, L. A. T. Machado,
1654 G. Bisht, R. Knox, and R. L. Bras, Impact of deforestation in the Amazon basin on
1655 cloud climatology, *PNAS*, 106(10), 3670–3674, doi:10.1073/pnas.0810156106, 2009.
- 1656 Wang, J., R. L. Bras, and E. Eltahir, The impact of observed deforestation on the
1657 mesoscale distribution of rainfall and clouds in Amazonia, *J Hydrometeorol*, 1(3),
1658 267–286, 2000.



- 1659 Wang, S., A. H. Sobel, and Z. Kuang, Cloud-resolving simulation of TOGA-COARE
1660 using parameterized large-scale dynamics, *J Geophys Res-Atmos*, 118(12), 6290–
1661 6301, doi:10.1002/jgrd.50510, 2013.
- 1662 Wang, Y. P., and R. Leuning, A two-leaf model for canopy conductance, photosynthesis
1663 and partitioning of available energy I:, *Agr Forest Meteorol*, 91(1-2), 89–111,
1664 doi:10.1016/S0168-1923(98)00061-6, 1998.
- 1665 Washington, R., R. James, H. Pearce, W. M. Pokam, and W. Moufouma-Okia, Congo
1666 Basin rainfall climatology: can we believe the climate models? *Philos T R Soc B*,
1667 368(1625), 20120296–20120296, doi:10.1098/rstb.2012.0296, 2013.
- 1668 Wehr, R., R. Commane, J. W. Munger, J. B. McManus, D. D. Nelson, M. S. Zahniser, S.
1669 R. Saleska, and S. C. Wofsy, Dynamics of canopy stomatal conductance,
1670 transpiration, and evaporation in a temperate deciduous forest, validated by carbonyl
1671 sulfide uptake., 1–17, doi:10.5194/bg-2016-365, 2016.
- 1672 Werth, D., and R. Avissar, The local and global effects of Amazon deforestation, *J*
1673 *Geophys Res-Atmos*, 107(D20), 8087, doi:10.1029/2001JD000717, 2002.
- 1674 Wills, R. C., M. P. Byrne, and T. Schneider, Thermodynamic and dynamic controls on
1675 changes in the zonally anomalous hydrological cycle, *Geo Res Letters*, 43(9), 4640–
1676 4649, doi:10.1002/2016GL068418, 2016.
- 1677 Wright, J. S., R. Fu, J. R. Worden, S. Chakraborty, N. E. Clinton, C. Risi, Y. Sun, and L.
1678 Yin, Rainforest-initiated wet season onset over the southern Amazon, *PNAS*,
1679 114(32), 8481–8486, doi:10.1073/pnas.1621516114, 2017.
- 1680 Wu, C.-M., B. Stevens, and A. Arakawa, What Controls the Transition from Shallow to
1681 Deep Convection? *J Atmos Sci*, 66(6), 1793–1806, doi:10.1175/2008JAS2945.1,
1682 2009.
- 1683 Xu, X., D. Medvigy, J. S. Powers, J. M. Becknell, and K. Guan, Diversity in plant
1684 hydraulic traits explains seasonal and inter-annual variations of vegetation dynamics
1685 in seasonally dry tropical forests, *New Phytologist*, 1–16, doi:10.1111/nph.14009,
1686 2016.



- 1687 Yano, J. I., and R. S. Plant, Convective quasi-equilibrium, *Rev Geophys*, 50(4), RG4004,
1688 doi:10.1029/2011RG000378, 2012.
- 1689 Yin, L., R. Fu, E. Shevliakova, and R. E. Dickinson, How well can CMIP5 simulate
1690 precipitation and its controlling processes over tropical South America? *Climate*
1691 *dynamics*, 41(11-12), 3127–3143, doi:10.1007/s00382-012-1582-y, 2013.
- 1692 Yu, H., L. A. Remer, M. Chin, H. Bian, R. G. Kleidman, and T. Diehl, A satellite-based
1693 assessment of transpacific transport of pollution aerosol, *J Geophys Res-Atmos*,
1694 113(D14), doi:10.1029/2007JD009349, 2008.
- 1695 Zahn, E., N. L. Dias, A. Araújo, L. D. A. Sá, M. Sörgel, I. Trebs, S. Wolff, and A. Manzi,
1696 Scalar turbulent behavior in the roughness sublayer of an Amazonian forest, *Atmos.*
1697 *Chem. Phys*, 16(17), 11349–11366, doi:10.5194/acp-16-11349-2016, 2016.
- 1698 Zeng, N., and J. D. Neelin, A land-atmosphere interaction theory for the tropical
1699 deforestation problem, *J Climate*, 12(2-3), 857–872, 1999.
- 1700 Zeng, N., J. Neelin, K. Lau, and C. Tucker, Enhancement of Interdecadal Climate
1701 Variability in the Sahel by Vegetation Interaction, *Science*, 286(5444), 1537–1540,
1702 1999.
- 1703 Zeppel, M. J. B., J. D. Lewis, N. G. Phillips, and D. T. Tissue, Consequences of nocturnal
1704 water loss: a synthesis of regulating factors and implications for capacitance,
1705 embolism and use in models, *Tree Physiol*, 34(10), 1047–1055,
1706 doi:10.1093/treephys/tpu089, 2014.
- 1707 Zhang, K., de Almeida Castanho, A.D., Galbraith, D.R., Moghim, S., Levine, N.M., Bras,
1708 R.L., Coe, M.T., Costa, M.H., Malhi, Y., Longo, M. and Knox, R.G., The fate of
1709 Amazonian ecosystems over the coming century arising from changes in climate,
1710 atmospheric CO₂, and land use, *Global Change Biol*, 21(7), 2569–2587,
1711 doi:10.1111/gcb.12903, 2015.
- 1712 Zhang, Y. J., F. C. Meinzer, and J. Qi, Midday stomatal conductance is more related to
1713 stem rather than leaf water status in subtropical deciduous and evergreen broadleaf



- 1714 trees, *Plant Cell and Env*, 36(1), 149–158, doi:10.1111/j.1365-3040.2012.02563.x,
1715 2013.
- 1716 Zhang, Y., R. Fu, H. Yu, R. E. Dickinson, R. N. Juarez, M. Chin, and H. Wang, A
1717 regional climate model study of how biomass burning aerosol impacts land-
1718 atmosphere interactions over the Amazon, *Journal of Geophysical Research:*
1719 *Atmospheres (1984–2012)*, 113(D14), 1042, doi:10.1029/2007JD009449, 2008.
- 1720 Zhang, Y., R. Fu, H. Yu, Y. Qian, R. Dickinson, M. A. F. Silva Dias, P. L. da Silva Dias,
1721 and K. Fernandes, Impact of biomass burning aerosol on the monsoon circulation
1722 transition over Amazonia, *Geophys Res Lett*, 36(10), 1509,
1723 doi:10.1029/2009GL037180, 2009.
- 1724 Zhuang, Y., R. Fu, and J. A. Marengo, Seasonal variation of shallow-to-deep convection
1725 transition and its link to the environmental conditions over the Central Amazon, *J*
1726 *Geo Res: Atmo*, doi:10.1002/(ISSN)2169-8996, 2017.
- 1727
- 1728
- 1729



1730 Table 1. The surface friction velocity, subcloud layer height (where the minimum of
 1731 virtual potential temperature flux occurs), ratio of subcloud layer height and Obukhov
 1732 length, ratio of surface friction velocity and Deardorff convective velocity scale, and the
 1733 total number of identified clouds for 12 time instants in each case.

Case	S3	S2	S1	CTL	R1	R2	R3
$u_* u_*$ [m s ⁻¹]	0.07	0.14	0.21	0.28	0.35	0.42	0.56
z_i [m]	590	590	590	590	590	610	630
z_i / L	392. 1	49.0	14.5	6.1	3.1	1.9	0.8
u_* / w_* u_* / w_*	0.10	0.20	0.30	0.40	0.50	0.60	0.79
N_{cloud}	2248	2229	2283	2302	2250	2703	2776

1734
 1735
 1736
 1737
 1738
 1739
 1740
 1741
 1742
 1743
 1744
 1745
 1746

1747 List of Figures

1748



1749 Figure 1: Snapshot of cloud cover over the Amazon basin (courtesy NASA, MODIS
1750 visible bands) in the dry season. Small clouds are shallow convective clouds, highlighting
1751 surface Bowen ratio changes between the river and the forest. At the bottom right, the
1752 deep convective cells, does not follow the surface heterogeneity (and is much larger in
1753 scale).Figure 1: Snapshot of cloud cover over the Amazon basin (courtesy NASA,
1754 MODIS visible bands) in the dry season. Small clouds are shallow convective clouds,
1755 highlighting surface Bowen ratio changes between the river and the forest. At the bottom
1756 right, the deep convective cells, does not follow the surface heterogeneity (and is much
1757 larger in scale).

1758 Figure 2: Diurnal cycle in local hour of dry (red) and wet (blue) season observations of
1759 precipitation at K34, near Manaus, along with their standard deviation averaged across
1760 years 2010-2014.

1761 Figure 3: Response of tropically-averaged free tropospheric temperature between 700mb
1762 and 200mb to El Niño Southern Oscillation (choosing the ENSO 3.4 index)

1763 Figure 4: Seasonal variations in Evapotranspiration (ET) from WECANN, Precipitation
1764 (Precip) based on GPCP, Net Radiation (Rn) from CERES and Gross Primary Production
1765 (GPP) based on WECANN informed by Solar-Induced Fluorescence (SIF) over the wet
1766 part of the Amazon (top left), the Savanna region of Brazil (top right), over Indonesia
1767 (bottom left) and over the Congo basin (bottom right).

1768 Figure 5: Seasonality of Precipitation based on GPCP in the tropics in December-
1769 January-February (a), March-April-May (b), June-July-August (c), and September-
1770 October-November (SON) and its latitudinal average (e).

1771 Figure 6: same as Figure 5 but for Gross Primary Production (GPP)

1772 Figure 7: same as Figure 5 for latent heat flux LE

1773 Figure 8: same as Figure 5 for sensible heat flux H

1774 Figure 9: same as Figure 5 for evaporative fraction (EF), the ratio of LE to H+LE.

1775 Figure 10: same as Figure 5 for sea-level surface moist static energy flux, the sum of
1776 sensible heat flux H and latent heat flux

1777 Figure 11: Schematic showing the vertical structure of light and water limitations in a
1778 tropical forest.



1779 Figure 12: Climatology of the diurnal cycle of leaf water potential and top soil water
1780 potential in the dry and wet seasons in Caxiuana, Brazil simulated by the Community
1781 Land Model (CLM) with plant hydraulics.

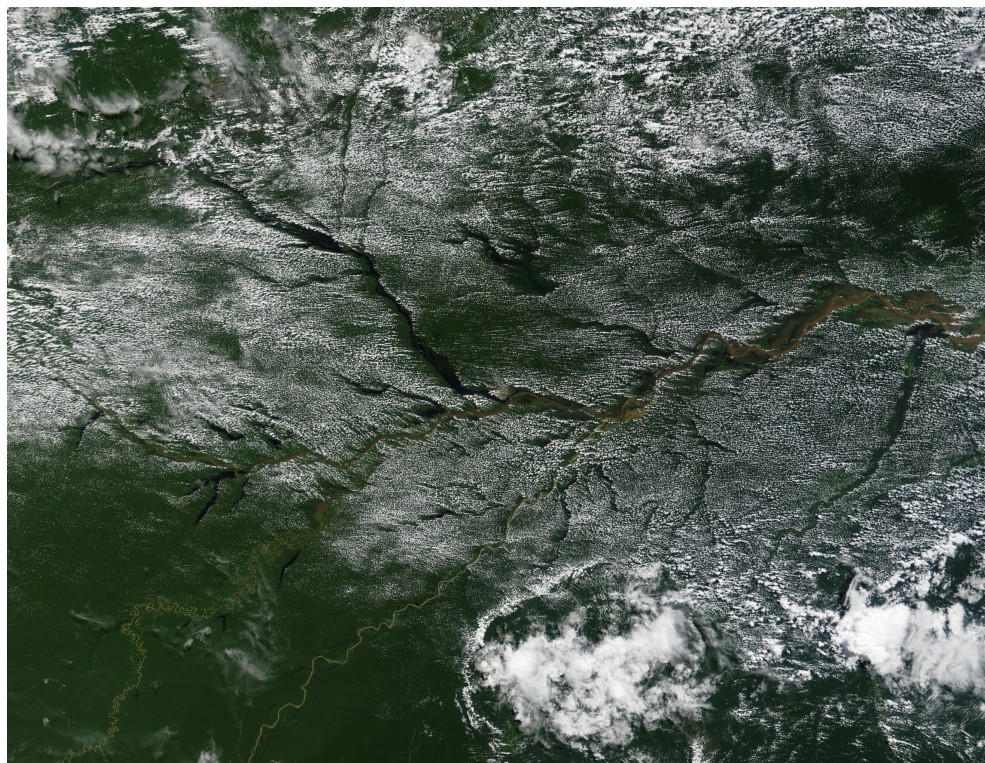
1782 Figure 13: Mesoscale heterogeneity impact on cloud generation. a) Typical perspective
1783 regarding the impact of deforestation and clearings generating deep convective clouds
1784 and b) more realistic impact, in terms of mostly a modification of shallow convection
1785 cloud cover, impacting radiation more than precipitation.

1786 *Figure 15:* (a) Schematic of the key elements of the convective margins framework as
1787 applied along an inflow path across northeastern South America. The solid blue and
1788 black lines are precipitation and vertically-integrated moisture, while dashed blue line
1789 corresponds to precipitation smeared out by transients. Adapted from Figure 2 of Lintner
1790 and Neelin (2009). (b) Rainfall longitudinal transects from the Climate Anomaly
1791 Monitoring System (CAMS) raingauge-derived precipitation data for September-
1792 October-November for the period 1950-2000 for El Niño (red), La Niña (blue), and all
1793 (black) years, averaged over 3.75°S-1.75°S. From Figure 4b of Lintner and Neelin
1794 (2007).

1795 Figure 16: adapted from Schäfli et al. (2012)

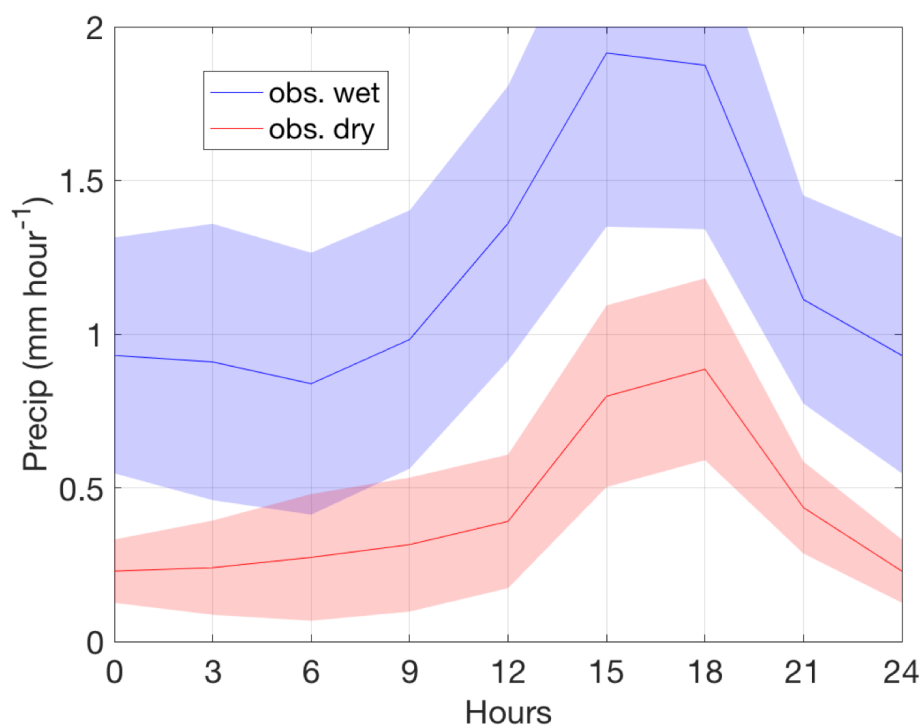
1796 Figure 18: Land-atmosphere feedback strength (change in the variance due to the
1797 feedback) between Precipitation and ET (top) and Photosynthetically Active Radiation
1798 (PAR) (bottom) based on recent metric developed by Green et al. [2017] using a
1799 multivariate Granger causality approach.

1800



1801

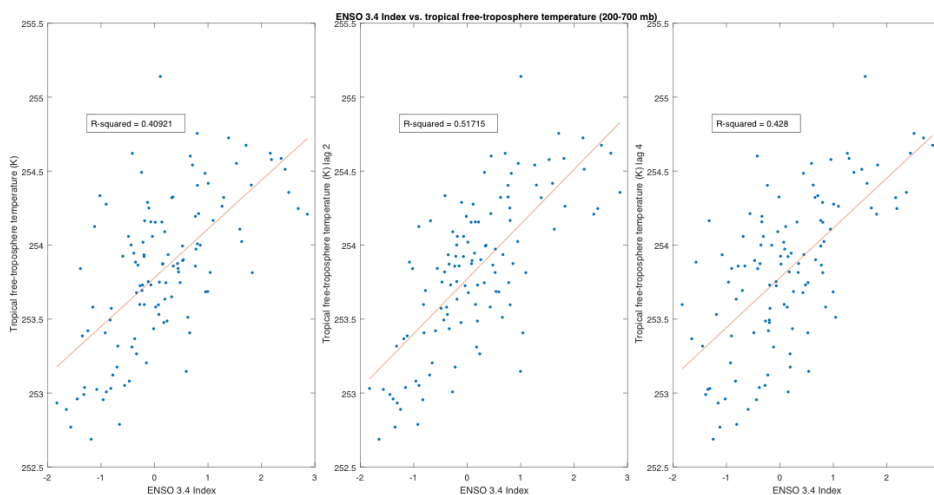
1802 Figure 1: Snapshot of cloud cover over the Amazon basin (courtesy NASA, MODIS visible
1803 bands) in the dry season. Small clouds are shallow convective clouds, highlighting surface Bowen
1804 ratio changes between the river and the forest. At the bottom right, the deep convective cells, does
1805 not follow the surface heterogeneity (and is much larger in scale).



1806

1807 Figure 2: Diurnal cycle in local hour of dry (red) and wet (blue) season observations of
1808 precipitation at K34, near Manaus, along with their standard deviation averaged across years
1809 2010-2014.

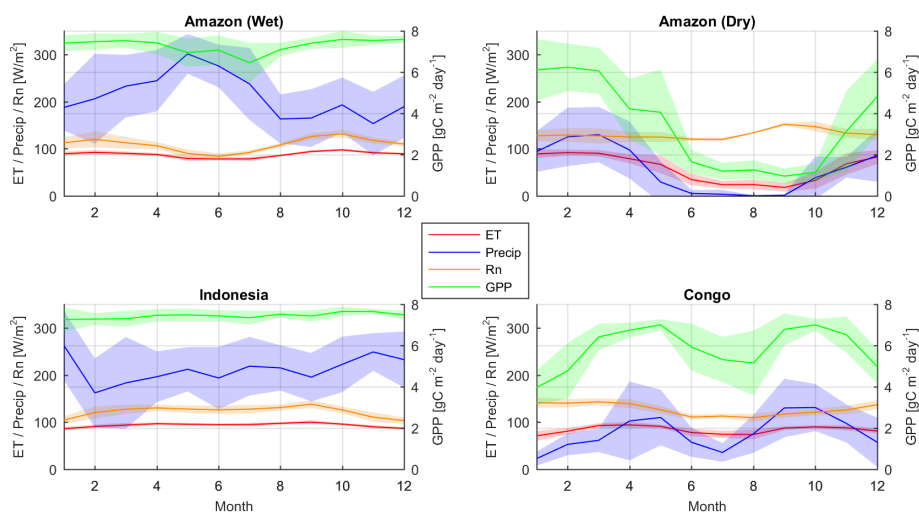
1810



1811

1812 Figure 3: Response of tropically-averaged free tropospheric temperature between 700mb and
 1813 200mb to El Niño Southern Oscillation (choosing the ENSO 3.4 index) with either no lag (left) or
 1814 2-month lag (middle) or 4-month lag (right)

1815



1816

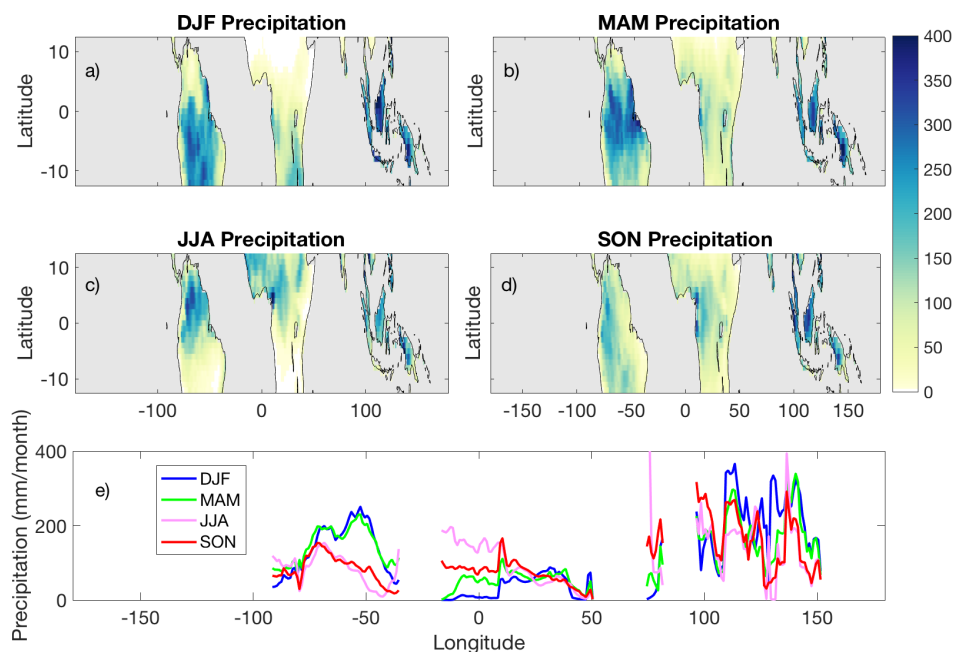
1817 Figure 4: Seasonal variations in Evapotranspiration (ET) from WECANN, Precipitation
 1818 (Precip) based on GPCP, Net Radiation (Rn) from CERES and Gross Primary Production (GPP)
 1819 based on WECANN informed by Solar-Induced Fluorescence (SIF) over the wet part of the
 1820 Amazon (top left), the Savanna region of Brazil (top right), over Indonesia (bottom left) and over



1821 the Congo basin (bottom right).

1822

1823

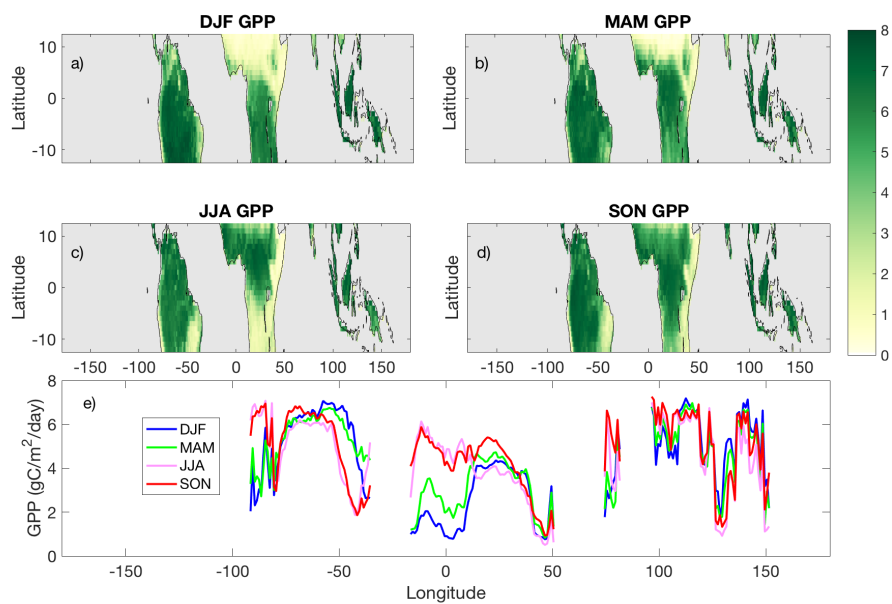


1824

1825 Figure 5: Seasonality of Precipitation based on GPCP in the tropics in December-
1826 January-February (a), March-April-May (b), June-July-August (c), and September-
1827 October-November (SON) and its latitudinal average (e).



1828

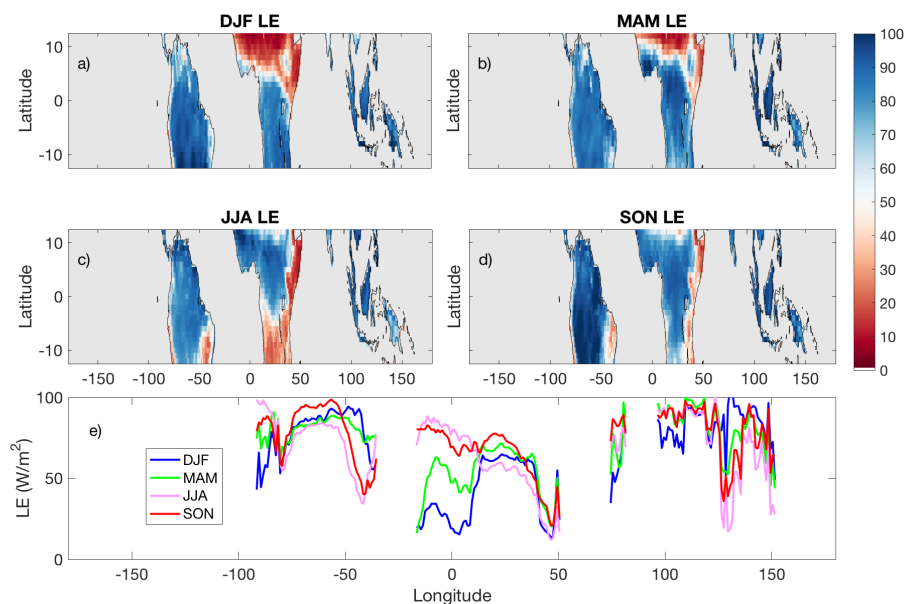


1829

1830 Figure 6: same as Figure 5 but for Gross Primary Production (GPP)

1831

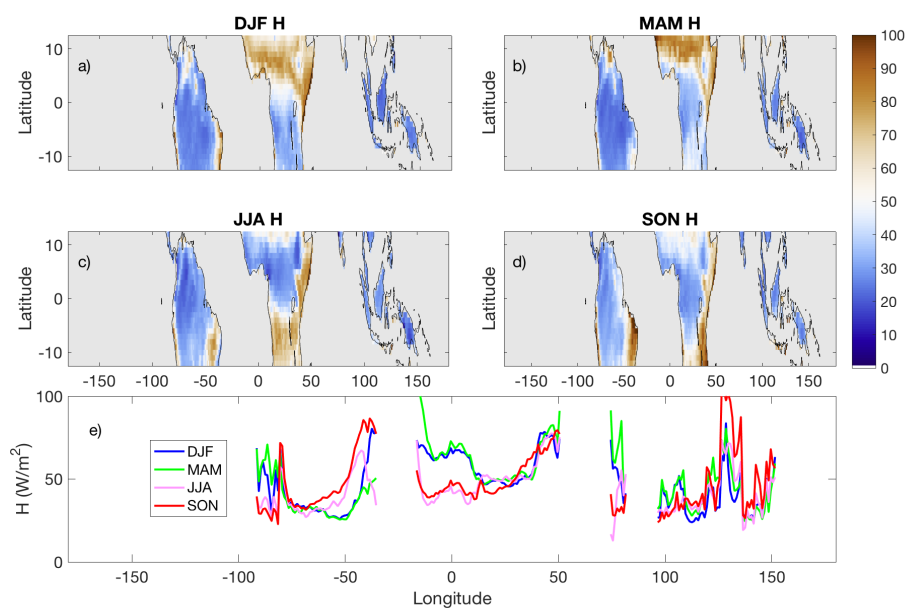
1832



1833

1834 Figure 7: same as Figure 5 for latent heat flux LE

1835



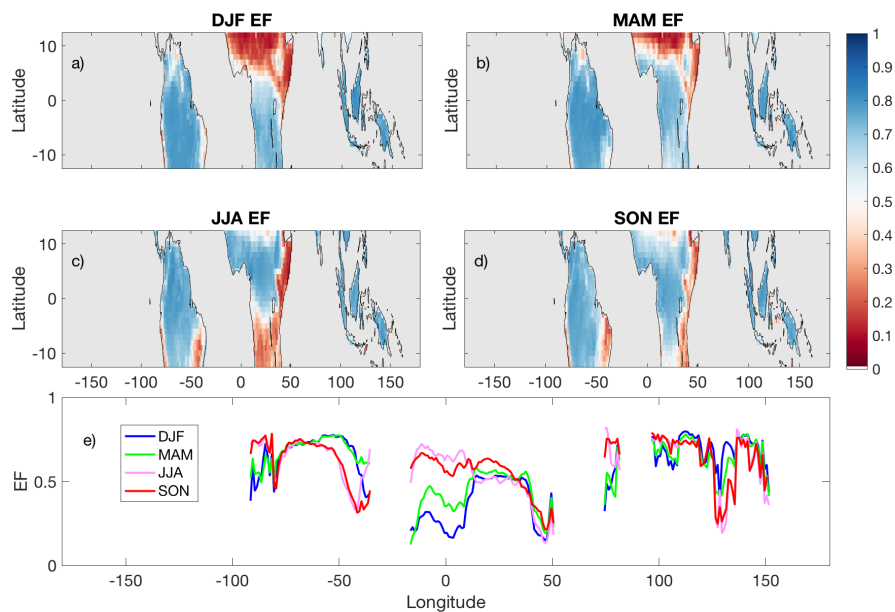
1836



1837 Figure 8: same as Figure 5 for sensible heat flux H

1838

1839



1840

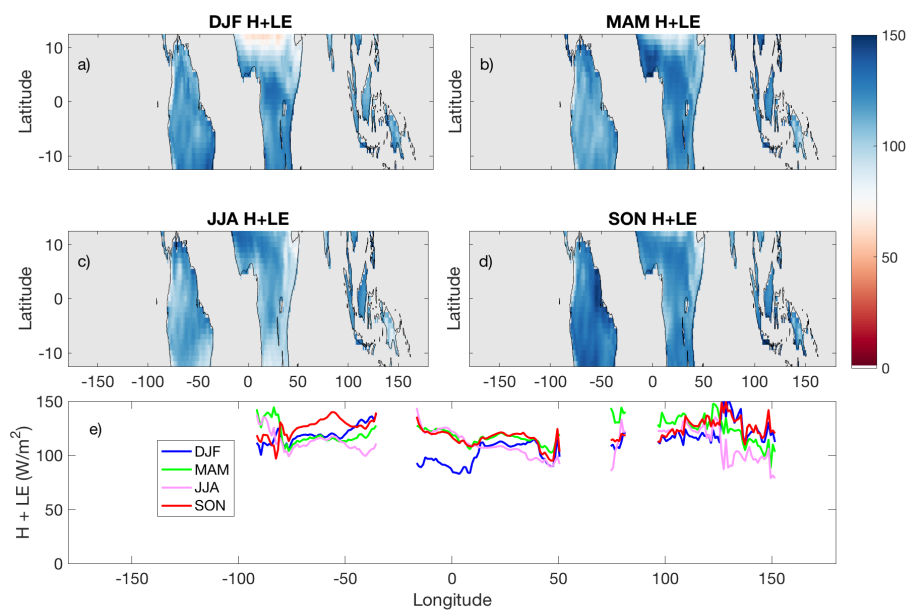
1841 Figure 9: same as Figure 5 for evaporative fraction (EF), the ratio of LE to H+LE.

1842

1843

1844

1845



1846

1847 Figure 10: same as Figure 5 for sea-level surface moist static energy flux, the sum of sensible
1848 heat flux H and latent heat flux

1849

1850

1851

1852



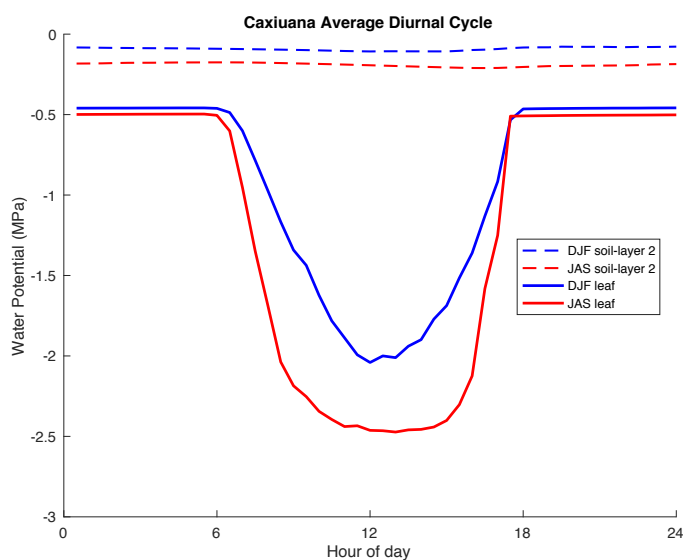
1853



1854 Figure 11: Schematic showing the vertical structure of light and water limitations in a tropical
 1855 forest.

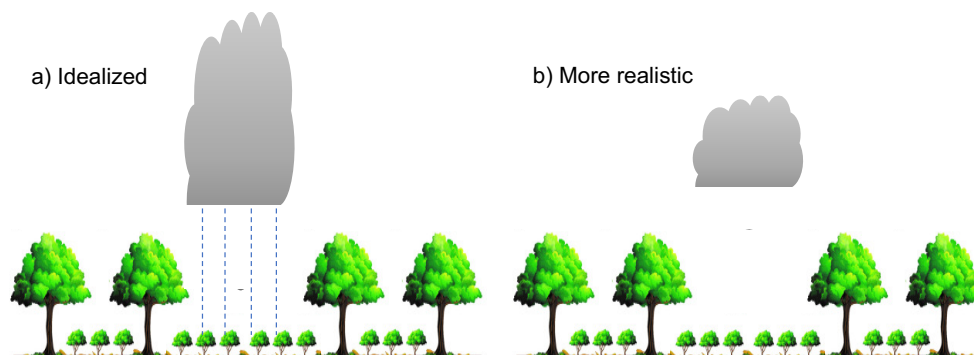
1856

1857



1858

1859 Figure 12: Climatology of the diurnal cycle of leaf water potential and top soil water
 1860 potential in the dry and wet seasons in Caxiuana, Brazil simulated by the Community
 1861 Land Model (CLM) with plant hydraulics.



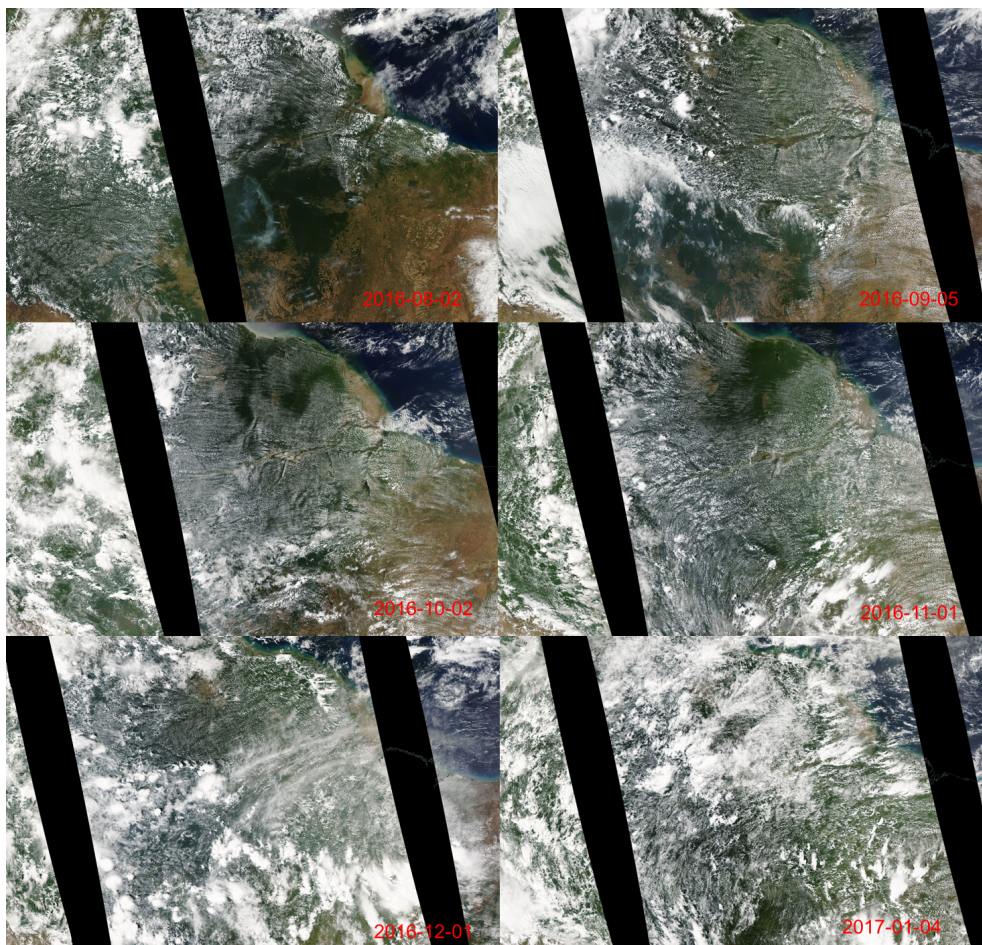
1862

1863 Figure 13: Mesoscale heterogeneity impact on cloud generation. a) Typical perspective
 1864 regarding the impact of deforestation and clearings generating deep convective clouds and b)
 1865 more realistic impact, in terms of mostly a modification of shallow convection cloud cover,
 1866 impacting radiation more than precipitation.



1867

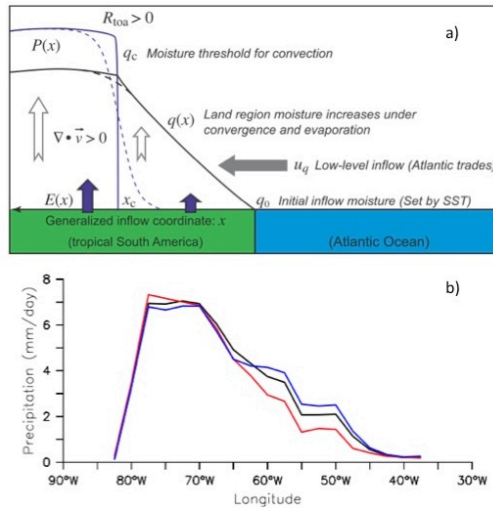
1868



1869

1870 Figure 14: MODIS visible image of the Northwestern Amazon as the basin transition into
1871 the wet season. In the dry season surface heterogeneity whether due to rivers, forest-
1872 deforested patches or land-ocean contrast are very clear. In the wet season those sharp
1873 gradients disappear as cloud cover mostly dominated by deep convection starts
1874 organizing at scales independent from the surface heterogeneity.

1875

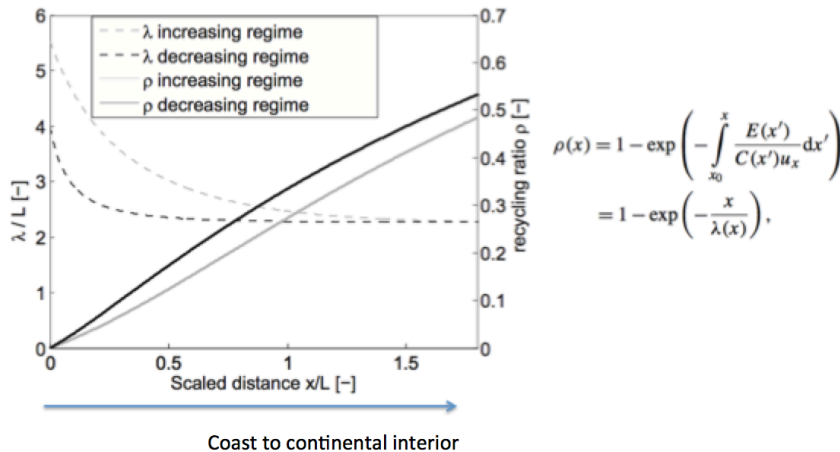


1876

1877 Figure 15: (a) Schematic of the key elements of the convective margins framework as applied along an
 1878 inflow path across northeastern South America. The solid blue and black lines are precipitation and
 1879 vertically-integrated moisture, while dashed blue line corresponds to precipitation smeared out by
 1880 transients. Adapted from Figure 2 of Lintner and Neelin (2009). (b) Rainfall longitudinal transects from
 1881 the Climate Anomaly Monitoring System (CAMS) raingauge-derived precipitation data for September-
 1882 October-November for the period 1950-2000 for El Niño (red), La Niña (blue), and all (black) years,
 1883 averaged over 3.75°S-1.75°S. From Figure 4b of Lintner and Neelin (2007).

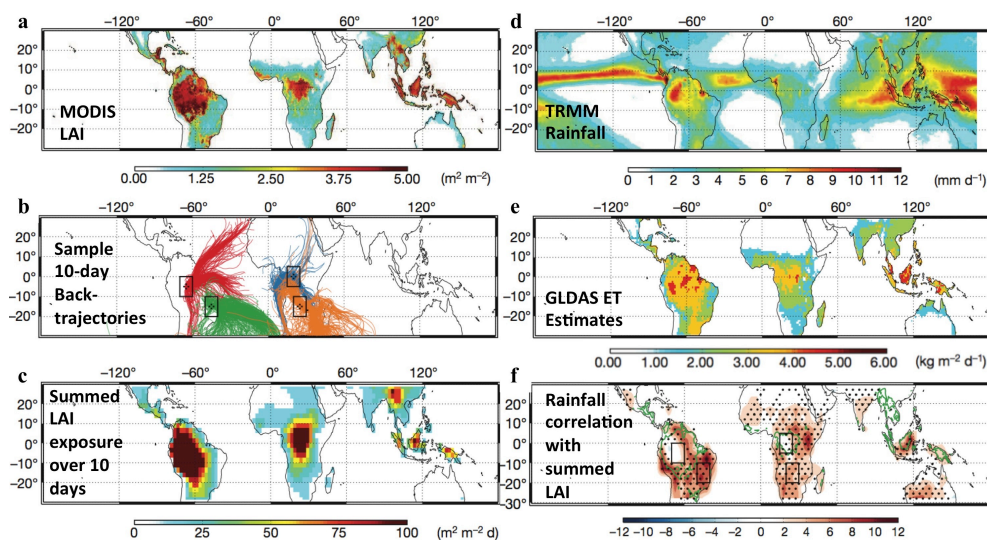
1884

1885



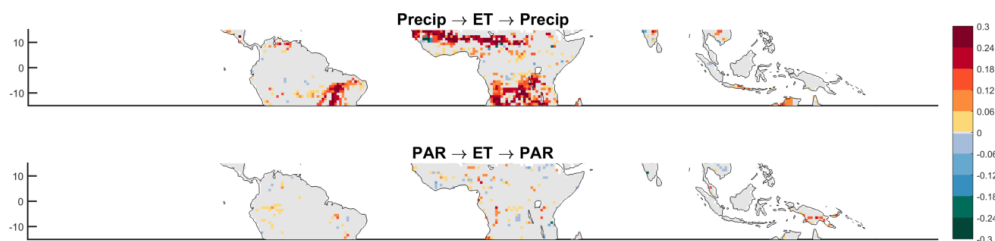
1886

1887 Figure 16: adapted from Schäfli et al. (2012)



1888
 1889 Figure 17: 10 day-backtrajectory analysis over several continental regions of the continental
 1890 tropics, along with LAI, mean TRMM estimated rainfall, and GLDAS ET estimates.

1891
 1892
 1893
 1894



1895
 1896 Figure 18: Land-atmosphere feedback strength (change in the variance due to the
 1897 feedback) between Precipitation and ET (top) and Photosynthetically Active Radiation
 1898 (PAR) (bottom) based on recent metric developed by Green et al. [2017] using a
 1899 multivariate Granger causality approach.

1900
 1901
 1902